



Simulating glacier lake outburst floods (GLOFs) with a two-phase/layer debris flow model considering fluid-solid flow transitions

Meyrat, G ; Munch, J ; Cicoira, Alessandro ; McArdell, B ; Müller, C R ; Frey, Holger ; Bartelt, P

Abstract: Glacier lake outburst floods (GLOFs) initiate with the rapid outburst of a glacier lake, endangering downstream populations, land, and infrastructure. The flow initiates as a mud flow; however, with the entrainment of additional solid material, the flood will often transform into a debris flow. As the run-out slope flattens, the coarse solid material deposits and the flow de-waters. The flow transforms back into a muddy, hyperconcentrated flow of fine sediments in suspension. These flow transitions change the flow composition dramatically and influence both the overall mass balance and flow rheology of the event. In this paper, we apply a two-phase/layer model to simulate flow transitions, solid–fluid phase separations, entrainment, and run-out distances of glacier lake outburst floods. A key feature of the model is the calculation of dilatant actions in the solid–fluid mixture which control flow transitions and phase separations. Given their high initial amount of fluid within the flow, GLOFs are sensitive to slope changes inducing flow transitions, which also implies changes in the flow rheology. The changes in the rheology are computed as a function of the flow composition and do not need any adaptation by ad-hoc selection of friction coefficients. This procedure allows the application of constant rheological input parameters from initiation to run-out. Our goal is to increase the prediction reliability of debris flow modeling. We highlight the problems associated with initial and boundary (entrainment) conditions. We test the new model against the well-known Lake 513 (Peru, 2010), Lake Palcacocha (Peru, 1941), and Lake Uchitel in the Aksay Valley (Kyrgyzstan) GLOF events. We show that flow transition modeling is essential when studying areas that have significant variations in slope.

DOI: <https://doi.org/10.1007/s10346-023-02157-w>

Posted at the Zurich Open Repository and Archive, University of Zurich

ZORA URL: <https://doi.org/10.5167/uzh-252861>

Journal Article

Published Version



The following work is licensed under a Creative Commons: Attribution 4.0 International (CC BY 4.0) License.

Originally published at:

Meyrat, G; Munch, J; Cicoira, Alessandro; McArdell, B; Müller, C R; Frey, Holger; Bartelt, P (2023). Simulating glacier lake outburst floods (GLOFs) with a two-phase/layer debris flow model considering fluid-solid flow transitions. *Landslides*:Epub ahead of print.

DOI: <https://doi.org/10.1007/s10346-023-02157-w>



Simulating glacier lake outburst floods (GLOFs) with a two-phase/layer debris flow model considering fluid-solid flow transitions

Abstract Glacier lake outburst floods (GLOFs) initiate with the rapid outburst of a glacier lake, endangering downstream populations, land, and infrastructure. The flow initiates as a mud flow; however, with the entrainment of additional solid material, the flood will often transform into a debris flow. As the run-out slope flattens, the coarse solid material deposits and the flow de-waters. The flow transforms back into a muddy, hyperconcentrated flow of fine sediments in suspension. These flow transitions change the flow composition dramatically and influence both the overall mass balance and flow rheology of the event. In this paper, we apply a two-phase/layer model to simulate flow transitions, solid–fluid phase separations, entrainment, and run-out distances of glacier lake outburst floods. A key feature of the model is the calculation of dilatant actions in the solid–fluid mixture which control flow transitions and phase separations. Given their high initial amount of fluid within the flow, GLOFs are sensitive to slope changes inducing flow transitions, which also implies changes in the flow rheology. The changes in the rheology are computed as a function of the flow composition and do not need any adaptation by ad-hoc selection of friction coefficients. This procedure allows the application of constant rheological input parameters from initiation to run-out. Our goal is to increase the prediction reliability of debris flow modeling. We highlight the problems associated with initial and boundary (entrainment) conditions. We test the new model against the well-known Lake 513 (Peru, 2010), Lake Palcacocha (Peru, 1941), and Lake Uchitel in the Aksay Valley (Kyrgyzstan) GLOF events. We show that flow transition modeling is essential when studying areas that have significant variations in slope.

Keywords Debris flow hazards · GLOFs · Two-layer model · Flow transition/phase separation · Entrainment/deposition · Debris flow rheology · Numerical modeling

Introduction

A longstanding problem in hazard engineering in mountainous regions is to accurately predict the possible inundation area of glacier lake outburst floods (GLOFs) (Emmer et al. 2022; Emmer 2017; Dunning et al. 2023; Medeu et al. 2022; Lliboutry 1977; Zheng et al. 2021; Richardson and Reynolds 2000). These are gravity-driven mixtures of water and granular sediments that can exhibit a wide range of different flow behaviors, depending on the initial (release) and boundary (entrainment) conditions, as well as on the terrain topography which controls the onset of solid deposition in the run-out zone and de-watering inducing subsequent flooding downstream (Westoby et al. 2014; Worni et al. 2014). GLOFs are a growing hazard due to the increasing amount of lakes forming close by retreating

glaciers (Shugar et al. 2020; Westoby et al. 2014). They are also very sensitive to changing climatic conditions including extreme rainfall events, sediment accumulations, and increasingly unstable slope conditions caused by ice melt and permafrost warming and thawing (Petraikov et al. 2016; Farinotti et al. 2015; Zheng et al. 2021; Emmer 2017). Because GLOFs can travel extreme distances, often in the order of magnitude of tens of kilometers (Richardson and Reynolds 2000; Worni et al. 2014), they can cause extensive damage in populated areas with little warning (Dunning et al. 2023).

The main difficulty in accurately predicting the travel velocity and run-out of GLOFs is that there is considerable uncertainty in the fluid/solid composition of a single event (Fig. 1). The fluid and solid contents of a GLOF event can vary dramatically, from around 10% for a mud flow to more than 60% for a granular debris flow (Hungre et al. 2014; Pierson 2005) (see Fig. 2). Often a GLOF will undergo flow transitions (Fig. 2) by depositing solid material on flatter slopes to turn into a flood, or eroding solid material on steeper slopes to turn into a debris flow (Worni et al. 2014). Flow transitions tend to maximize GLOF run-out, but are difficult to model because they involve the interplay between flow rheology, sediment entrainment, and terrain topography.

The inherent variability of flow regimes represents one of the largest sources of uncertainties in the modeling of GLOFs, with critical implications for hazard management. This idea was first formulated by Iverson (2003) who formulated the idea that the diversity of flow regimes cannot be modeled by a simplistic, single component flow rheology as the *rheology myth*. Even if the rheology of a specific flow regime (see Table 2, Pierson (2005)) is relatively well parameterized, the neighboring flow regimes, differing only in fluid and solid content, can require an entirely different parameterization. A common feature of this phenomena is the wide range of Coulomb friction values needed to model the correct run-out distance in practical case studies (Graf et al. 2019; Mikoš and Bezak 2021; Simoni et al. 2012) (see Fig. 2). This observation is well supported by real-size debris flow measurements at the Swiss Illgraben test site, which show a wide variation of Coulomb friction values and an explicit dependency of the basal shear on the fluid concentration in the flow (Meyrat et al. 2022; Meyrat 2007). Modern three-dimensional numerical schemes couple finite-strain elastoplasticity models to the conservation equations for mass and momentum in a relatively simple manner (Gaume et al. 2019, 2018). This combination allows for the set up of extremely complex events with a limited need for parameter calibration (Cicoira et al. 2022). However, this family of models is still in the development phase and is currently far away from practical applications from practitioners and authorities.

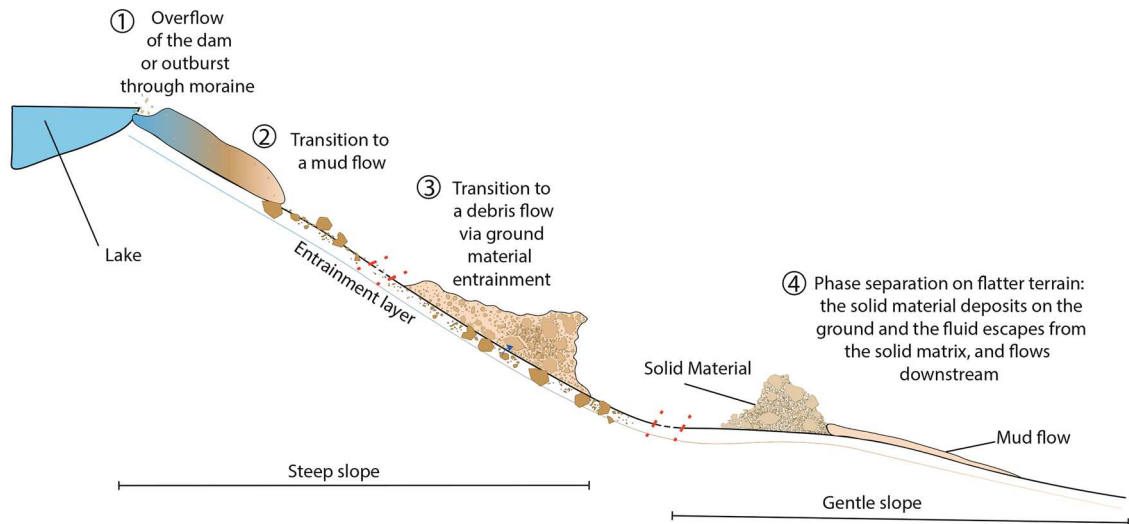


Fig. 1 Typical flow regime transitions during a GLOF event. The flow is initially a mud flow that can transform into a debris flow with the erosion of solid debris. If the slope becomes flatter, for example, in the run-out zone, the core of the debris flow deposits and stops. The fluid can separate from the solid matrix and continues to flow downstream in the form of a muddy or hyperconcentrated flow (Hungri et al. 2014). If the slope becomes steeper, the entire process might occur again. The red dashed lines in the figure (between stages 2–3 and 3–4) indicate a potentially large distance between the different flow regimes, where flow transitions could occur again depending on the sediment availability and terrain topography

It appears that the search for an accurate numerical model for GLOFs and other saturated granular flows begins with the introduction of a numerical model that can reproduce the flow composition and its complex spatio-temporal variability, not only from initiation to run-out, but also from the leading edge to the tail of the flow.

In this paper, we present the two-phase/layer extension of the *RAMMS::DEBRISFLOW* one-phase model developed at SLF (Ramms 2017; Frank et al. 2015). We apply this new model for the simulation of flow transitions and phase separations observed in three well-known GLOF case studies (Lake 513, Lake Palcacocha, and Aksay Valley). These flow transitions are responsible for the

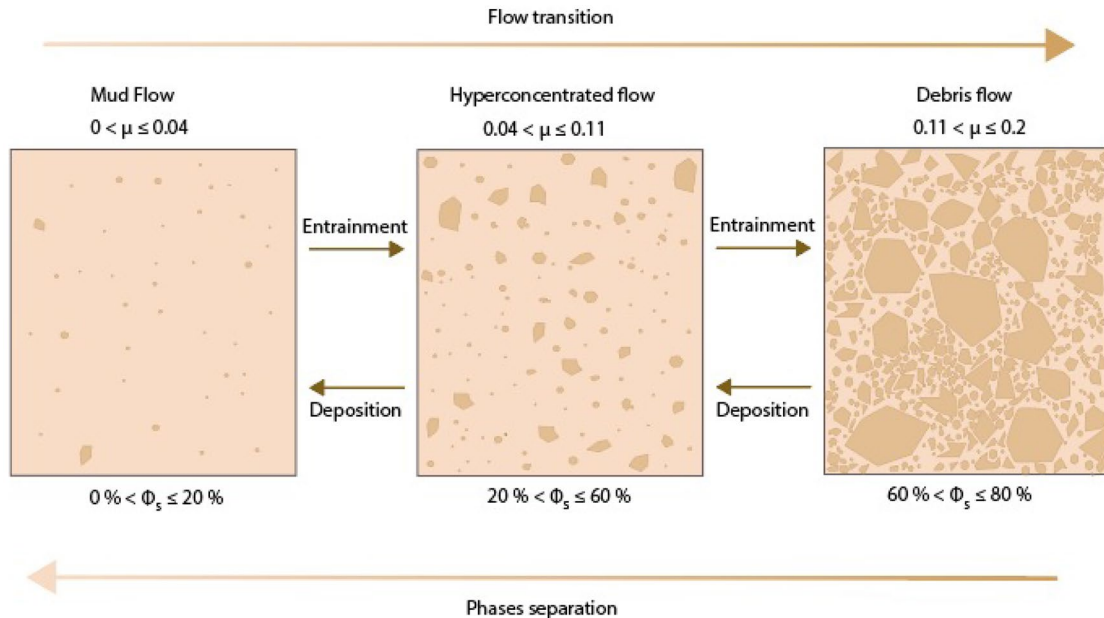


Fig. 2 Different flow types and their corresponding solid concentrations (ϕ_s) and rheologies (μ , Graf et al. 2019; Mikoš and Bezak 2021; Simoni et al. 2012). The corresponding values of ξ are not given, because they are still not well constrained

long-range flow mobility of the mass movements. To this end, we must address the entire complexity of GLOF dynamics, including release conditions, flow rheology, entrainment, and long-distance flow over complex terrain. Unlike many existing models that use a Darcy-like approximation to compute the fluid velocity (Iverson and George 2014; George and Iverson 2014; Pitman and Le 2005; Bouchut et al. 2016), we formulate a two-phase/layer model that contains an independent fluid phase in order to model de-watering and subsequent flooding. The Darcy approximation can be considered valid only for flows with high solid concentration, which is not necessarily the case when for GLOF-type events. Models which do not use a Darcy-like approximation to simplify the fluid momentum conservation equation (Pudasaini 2012; Pudasaini and Hutter 2007) are confronted with the mathematical problem of computing the momentum transfer between the solid and the fluid phases. Such approaches require the introduction of additional free parameters (up to three for instance, in the case of r.avaflow Pudasaini (2012)), which are difficult to calibrate and, therefore, problematic to use by practitioners. To overcome these problems, we adopt the method developed by Meyrat et al. (2022) and Meyrat (2007). We first calculate flow dilations in the matrix of coarse granular sediments as a function of the basal shear stress and the volumetric solid concentration. Based on this, we predict the fluid mass that exists in the interstitial pore space between the solid, granular debris. Solid flow dilations induce fluid mass transfers between the solid and fluid layers. These mass exchanges are associated with interlayer momentum transfers. We show that this entire procedure can be modeled with only one additional free parameter, Γ (Annex) Meyrat et al. (2022), which controls the mean dispersion/contraction time of the dilatant configuration. This parameter is calibrated by back-calculating natural events to maximize the accuracy of the results.

To test the model, we analyze three GLOF events. The first two events are the outburst floods of the Lake 513 in 2010 and the Lake Palcacocha in 1941, both located in Peru. Lake 513 experienced a major GLOF in 2010, when a 450,000 m^3 rock-ice avalanche impacted the lake, causing severe damages along the GLOF trajectory and in the city of Carhuaz (Carey et al. 2012; Schneider et al. 2014). The well-known Lake Palcacocha outburst in 1941 destroyed a large part of the city of Huaraz (Wegner et al. 2014; Mergili et al. 2020). The third event is the outburst flood of the Uchitel Lake in the Aksay valley

in Kyrgystan (Zaginaev et al. 2019a; Petrakov et al. 2020). All three events are well described in the literature (Carey et al. 2012; Schneider et al. 2014; Mergili et al. 2020; Somos-Valenzuela et al. 2016; Zaginaev et al. 2016, 2019a, b), providing us with valuable information and field data to validate, overturn, and evaluate the model results. The literature, supported by observations, indicates that all three events underwent flow regime transitions.

Before describing the model equations, we must address the salient problem of bed erosion. In GLOF events, the initial release volume may represent only a small fraction of the total volume—sometimes only 10% (Bindereif 2022; Vicari et al. 2021). This indicates the important role of erosion in predicting long-distance GLOF run-out. Flow regime transitions are dependent on the entrainment and deposition processes, coupled with the evolving head-tail structure of the event. Thus, we enter into a complex, mechanical feedback loop between debris flow structure, governed by rheology and mass balance (difference between entrainment and deposition). Erosion processes strongly depend on the internal solid concentration and, therefore, on the flow structure, which clearly depends on the availability of solid debris, and therefore erosion. In the past, such complexity was modeled by ad-hoc adjustments to the flow rheology (for example, by changing the friction coefficients along the flow path, see Table 2). Although we perform an *a posteriori* analysis with event back-calculations, our motivation is to establish a well-defined and general set of parameters for debris flows that undergo flow regime transitions with entrainment.

Model definitions and equations

We model debris flows with a two-dimensional, depth-averaged shallow water formulation. The model consists of two material components: a solid component (subscript s) consisting of coarse granular sediments (e.g., boulders, cobbles, and gravel) associated with a density ρ_s , and a fluid component (subscript f), hereafter referred to as the muddy fluid content, whose density is denoted by ρ_f (Fig. 3). The fluid component consists of water supersaturated with fine sediments that behave as suspended sediments (e.g., sand, silt, clay). Many models, for example, r.avaflow, Pudasaini (2012), treat coarse and fine sediments separately. In our formulation, the fine sediments are assumed to be suspended in the fluid. For this reason, the fluid density is assumed to be

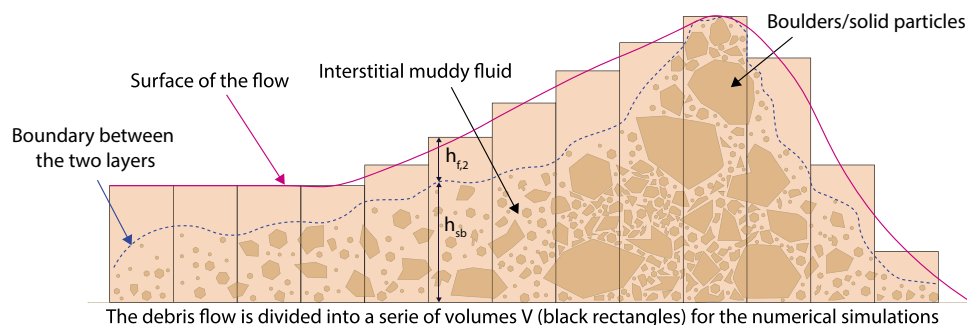


Fig. 3 Debris flow model. The flow consists of solid material in the form of boulders (granules) as well as two types of fluid. The bonded/interstitial fluid is located between the boulders and is fixed to the solid. The so-called free fluid is located above the granular solid/fluid mixture and can move independently

higher than water, approximately 1300 kg/m^3 (say). The coarse granular sediments form the solid phase. As the largest size of sediment in suspension is not well constrained in the literature (Uchida et al. 2021), we do not define the exact difference between suspended and non-suspended sediment size. It has been argued by Hooke and Iverson (1995) that particles larger than silt size are expected to contribute to the solid phase of debris flows. Others have demonstrated that the smallest particle size contributing to the solid phase in two-phase descriptions of flow is variable (Uchida et al. 2021).

We therefore employ a two-layer approach to define the movement of the debris flow (Bouchut et al. 2017; Pitman and Le 2005). The first layer (subscript 1) contains the granular solid material and a part of the fluid. This layer is termed the mixture layer. The fluid is contained in the interstitial space between particles and is assumed to be bonded to the solid matrix. The second layer (subscript 2) is formed by the fluid, which can flow independently from the first layer. All the fluid which flows above the first layer is considered free, and subsequently, it can escape the matrix of solid particles, allowing debris flow de-watering and phase separation. Contrary to the approaches of Bouchut et al. (2017) and Pitman and Le (2005), we assume that the velocities of both fluid components (interstitial and free fluid) differ. This layer definition allows for the formulation of equations for the fluid phase (through the free fluid equations) without having to deal with the complex momentum transfer between the fluid and solid phases. Indeed, in the mixture layer, both solid and fluid are assumed to flow at the same speed. This model formulation allows us to describe highly complex momentum interactions via mass transfers associated with the dilations in the solid matrix. As a consequence, the number of model parameters is reduced.

To describe the motion of the three different components (solid, interstitial fluid, free fluid), we need a system of three depth-averaged mass balance equations (Wang et al. 2004),

$$\frac{\partial h_1}{\partial t} + \vec{\nabla} \cdot (h_1 \vec{v}_1) = \left[\frac{\rho_f}{\rho_s} \right] Q_e + \left[\frac{\rho_e}{\rho_s} \right] E_1 \quad \text{solid and inter-granular fluid} \quad (1)$$

$$\frac{\partial h_{f,1}}{\partial t} + \vec{\nabla} \cdot (h_{f,1} \vec{v}_1) = Q_e + \left[\frac{\rho_e - \rho_f}{\rho_f - \rho_s} \right] E_1 \quad \text{inter-granular fluid} \quad (2)$$

$$\frac{\partial h_{f,2}}{\partial t} + \vec{\nabla} \cdot (h_{f,2} \vec{v}_2) = -Q_e \quad \text{second layer, free fluid} \quad (3)$$

where $h_{f,i}$ is the fluid content of the i -th layer and \vec{v}_i its velocity (see Figs. 3 and 4). h_1 is a pseudo-variable used to simplify the conservation equations (see next), E_1 is the erosion rate, Q_e is the fluid mass exchange due to the dilatant action of the solid matrix, ρ_e is the density of the entrained material, and $\vec{\nabla}$ is the divergence operator in Cartesian coordinates.

As the mixture layer density is neither constant nor uniform, it is convenient to introduce the variable h_1 , which is defined as the mixture layer mass, M_1 (per unit of area), normalized by the solid density ρ_s :

$$h_1 = \frac{M_1}{\rho_s} = \frac{\rho_s h_s + \rho_f h_{f,1}}{\rho_s} = h_s + \frac{\rho_f}{\rho_s} h_{f,1} \quad (4)$$

where h_s represents the volume of the solid in the first layer (per unit area). With the introduction of this variable, we obtain a system of depth-averaged equations that can be defined by constant density and therefore be solved using existing shallow water solvers. For more details about the numerical scheme, see Meyrat et al. (2022). The *density* associated with the variable h_1 is ρ_s , which is constant and uniform. Importantly, the variable h_1 is without physical meaning and is introduced to mathematically simplify the mass and momentum balance equations. In this paper, the physical first layer height will be noted h_{sb} and is the sum of both first layer components (see Figs. 3 and 4):

$$h_{sb} = h_s + h_{f,1}. \quad (5)$$

The equations relevant for the mixture layer (Eqs. 1 and 2) contain the erosion rate, denoted by E_1 . To compute the erosion rate, we adapted the single component model proposed by Frank et al. (2015, 2017) into the two-layer model. In the modified model, the erosion rate E_1 is no longer uniform nor constant as in Frank et al. (2015, 2017), but a function of the flow composition. If E_s represents

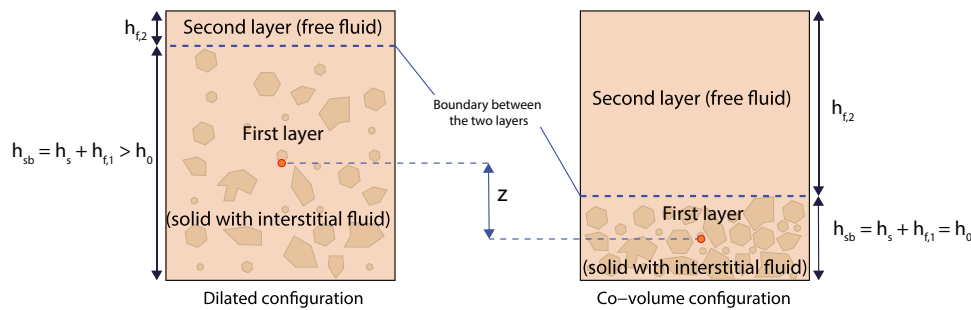


Fig. 4 Two different debris flow configurations consisting of equal amounts of solid and fluid masses. The left configuration is in a dilated configuration, occurring while flowing. The right configuration is the reference configuration, called the co-volume configuration, typically occurring when the flow is at rest. The different heights and other physical parameters are depicted in Meyrat et al. (2022). We define three variables associated with the solid mass: h_s , h_0 , and h_{sb} . The height h_s is the volume of the solid particles in the flow, h_0 represents the reference height of the non-dilated mass, we call it the co-volume (It is different from h_s because we consider that, even in the non-dilated configuration, the void space is not zero), whereas h_{sb} represents the dilated height of the solid mass, "Model definitions and equations"

the erosion rate for a completely solid flow and E_f for a completely fluid flood, the erosion rate E_1 is expressed under the assumption that erosion rates vary linearly between the two phases:

$$E_1(\phi_s) = \phi_s E_s + (1 - \phi_s) E_f \quad (6)$$

where ϕ_s and ϕ_f are the first layer's volumetric solid and fluid fraction, respectively. They are defined as follows:

$$\phi_s = \frac{h_s}{h_s + h_{f,1}} = \frac{h_s}{h_{sb}}; \quad \phi_f = 1 - \phi_s = \frac{h_{f,1}}{h_{sb}}. \quad (7)$$

Erosion rates for debris flows have been calibrated with field events, and values for specific soil-types are available (see Frank et al. (2015, 2017)). However, the separation between E_s and E_f is difficult to describe (non-linear) and therefore complicated to calibrate, partially due to a lack of experimental data. Therefore, we set as a first approximation that E_s is some multiple of E_f . This reduces the number of free parameters in the model. Indeed, in this study, we prefer to describe the entrainment with a simple parametrization, with fewer model parameters and a simple physical interpretation rather than develop sophisticated but complex models (Cicoira et al. 2022). This approach facilitates the application to real events (and as we show in the results is sufficient to obtain realistic results). However, a better understanding of the erosion processes, more specifically the interdependency on the composition of the flowing debris, would help clarify the link between the solid and fluid erosion rates. The erosion rate is specified in the slope-perpendicular direction. Therefore, the model includes both downward erosion processes, but also lateral erosion from channel sides. Erosion begins when the shear stress is larger than some limit value. Because we adopt a Voellmy-type rheology, the basal shear stress is both a function of the normal stress and the velocity of the flow.

The free fluid can erode ground material only if the first layer height is zero (in fact, smaller than a typical granule size value, which we assume to be around 5 cm; see Annex). In the alternative case, in which the free fluid flows above the mixture layer, the free fluid layer does not touch the ground (it is, by definition, flowing above the first layer). In this case, the eroded material is directly inserted into the mixture layer (because the second layer cannot possess solid material). This is the reason why E_1 is absent of Eq. 3. The erosion depth of the second layer is also computed using the model introduced by Frank et al. (2015, 2017), with an erosion rate corresponding to E_f . The shear stress used in the erosion depth computation (Frank et al. 2015, 2017) is the total shear stress, i.e., the sum of the shear stress of both layers. We also added a critical erosion velocity, $v_c = 0.5 \text{ m/s}$ (see Annex), which is the velocity threshold for erosion to begin.

The right-hand side of the mass conservation equations (Eqs. 1–3) contains the term Q_e (Meyrat et al. 2022), which is the fluid mass exchange rate between the inter-granular and free fluid. As stated above, the mass exchanges between the mixture layer and free fluid result from the dilatant actions of the solid particles in the debris flow (Meyrat et al. 2022; Iverson 1997, 2005). Under interactions with the rough bed of the channel, the solid matrix can dilate (Reynolds 1885; Buser and Bartelt 2009) and raise its center of mass from the co-volume configuration (whose height is noted h_0 , right sketch on Fig. 4) to a dilated one (left sketch on Fig. 4). Under

dilation, the void space between the particle increases (Bartelt et al. 2016), and free fluid fills this additional volume and is transformed into interstitial fluid. The inverse process occurs during the contraction of the solid matrix, for instance, when the flow reaches the run-out zone. The mass exchange rate is completely defined by the movement of the solid matrix center of mass (and the amount of fluid in the second layer). Therefore, the dilatancy governs the evolution of the first layer density, ρ_1 , which can vary even if the solid mass (h_s) is conserved, throughout the inter-granular fluid concentration $\phi_f = (1 - \phi_s)$ (and then dilatancy) (Eq. 7):

$$\rho_1 = \frac{M_1}{h_{sb}} = \frac{\rho_s h_s + \rho_f h_{f,1}}{h_{sb}} = \phi_s \rho_s + (1 - \phi_s) \rho_f. \quad (8)$$

Dilatant actions in the mixture layer are exploited to simulate de-watering and phase separations. Indeed, when the debris flow reaches the run-out zone, the flow decelerates, and the frictional shear works as well, which implies that the energy input coming from shearing is no longer sufficient to maintain the solid matrix in a dilated configuration. Consequently, the solid material contracts (the opposite of dilating), leading to an increase in friction and eventual deposition. During the collapse of the mixture layer, interstitial water is squeezed out and transformed into free fluid, which can escape from the solid matrix. For more details about the mathematical structure of the dilatancy theory, see Meyrat et al. (2022) and Meyrat (2007).

The variable h_1 is also used to simplify the two-dimensional, depth-averaged momentum balance equations (Wang et al. 2004; Savary and Zech 2007; Mandli 2011):

$$\begin{aligned} \partial_t(h_1 \vec{v}_1) + \vec{\nabla} \cdot \left(h_1 \vec{v}_1 \otimes \vec{v}_1 + \frac{gh_1^2}{2} I \right) + gh_1 \vec{\nabla} \left(b + \frac{\rho_f}{\rho_s} h_{f,2} \right) &= -\frac{\vec{\tau}_1}{\rho_s} + \frac{\rho_f}{\rho_s} \vec{P} \\ \partial_t(h_{f,2} \vec{v}_2) + \vec{\nabla} \cdot \left(h_{f,2} \vec{v}_2 \otimes \vec{v}_2 + \frac{gh_{f,2}^2}{2} I \right) + gh_{f,2} \vec{\nabla} (b + h_{sb}) &= -\frac{\vec{\tau}_2}{\rho_f} - \vec{P} \end{aligned}$$

The vectors \vec{v}_1 and \vec{v}_2 represent the velocity of the first and second layers, respectively. The left-hand sides of Eq. (9) are the total variation of the momentum with respect to time, including the effect of gravity and the influence of each layer on the other (Savary and Zech 2007; Mandli 2011). The right-hand side represents the change in momentum due to external forces (excluding gravity). The vector \vec{P} is the rate of momentum exchange associated with the

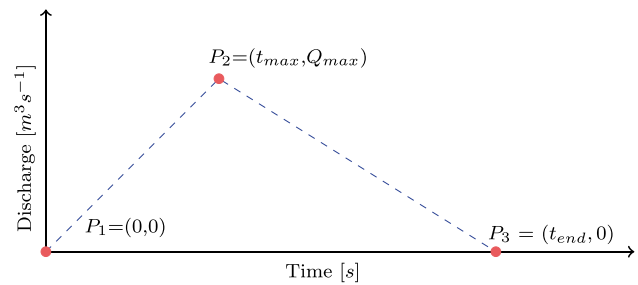


Fig. 5 The hydrograph is defined by three points. Q_{max} and t_{max} are defined according to field works (Zaginaev et al. 2019a; Mergili et al. 2020; Carey et al. 2012), while t_{end} is computed with Eq. 15 to reach the total volume of the hydrograph

Table 1 Values of the input hydrograph parameters for the three case studies. The discharge of the Aksay Valley event is much lower, because it corresponds to a sub-glacial breaching process and not a wave that overtops the moraine dam or a moraine dam failure

Event	Total volume (m ³)	Peak discharge (m ³ /s)	Time of the peak discharge (s)	End time (s)
Lake 513	50,000	8333	2	12
Lake Palcacocha	10,000,000	20,000	20	1000
Aksay Valley	35,000	50	100	1400

mass exchange Q_e , and $\bar{\tau}_i$ corresponds to the shearing stress acting on the i -th layer. To compute the shearing forces, we use the two parameters (μ and ξ) Voellmy-formulation, which is well-known in natural hazard mitigation practice in Switzerland and elsewhere (Mikoš and Bezak 2021; Simoni et al. 2012). In this simple model formulation, the Coulomb friction determines the debris flow run-out, as it defines the critical slope angle θ_c at which the flow begins to decelerate (Graf et al. 2019):

$$\tan \theta_c = \mu. \quad (9)$$

The hydraulic friction ξ controls the flow speed of the movement. It allows for steady flow states to exist in ideal conditions, for example, infinitely long slopes with constant angle. Thus, we can control the approximate run-out distance and steady flow velocity with only two parameters.

The debris flow rheology, $\bar{\tau}_i$, is not constant and uniform but a function of the flow composition (Iverson and Denlinger 2001). The friction decreases when increasing the volumetric fluid fraction of the flow (or equivalently when decreasing the flow density). This empirical assumption is supported by well-constrained field measurements from Illgraben (Meyrat et al. 2022; Schlunegger et al. 2009; Badoux et al. 2009; McArdell and Sartori 2020). In order to take the flow composition into account, let us define four frictional coefficients: ξ_s and μ_s , which describe the densest

configuration of the mixture, i.e., the co-volume, and μ_f and ξ_f describe the free fluid. As the free fluid layer is always entirely fluid, its coefficients do not evolve and are always the same. That is, μ_f and ξ_f are constants.

For the mixture layer, we compute the Coulomb and turbulent coefficients by partitioning according to the solid and fluid volumetric parts:

$$\mu_1(\phi_s) = \frac{h_s \mu_s + h_{f,1} \mu_f}{h_s + h_{f,1}} = \phi_s \mu_s + (1 - \phi_s) \mu_f = \phi_s \mu_s \quad (10)$$

$$\xi_1(\phi_s) = \frac{h_s \xi_s + h_{f,1} \xi_f}{h_s + h_{f,1}} = \phi_s \xi_s + (1 - \phi_s) \xi_f. \quad (11)$$

We assume that the Coulomb friction will be negligible if the flow is entirely composed of fluid, which means that $\mu_f = 0$ (Eq. 10). This assumption is justified by the fact that the critical slope angle (Eq. 9) is zero for a liquid flow. Once the frictional parameters $\mu_1(\phi_s)$ and $\xi_1(\phi_s)$ are evaluated accordingly to the flow composition, we use the Voelly-Salm model to compute the frictional resistance of the flow, i.e.,

$$\bar{\tau}_1 = \mu_1(\phi_s) N_1 \hat{e}_1 + \frac{\rho_1 g \|v_1\|^2}{\xi_1(\phi_s)} \hat{e}_1 \quad \text{First layer} \quad (12)$$

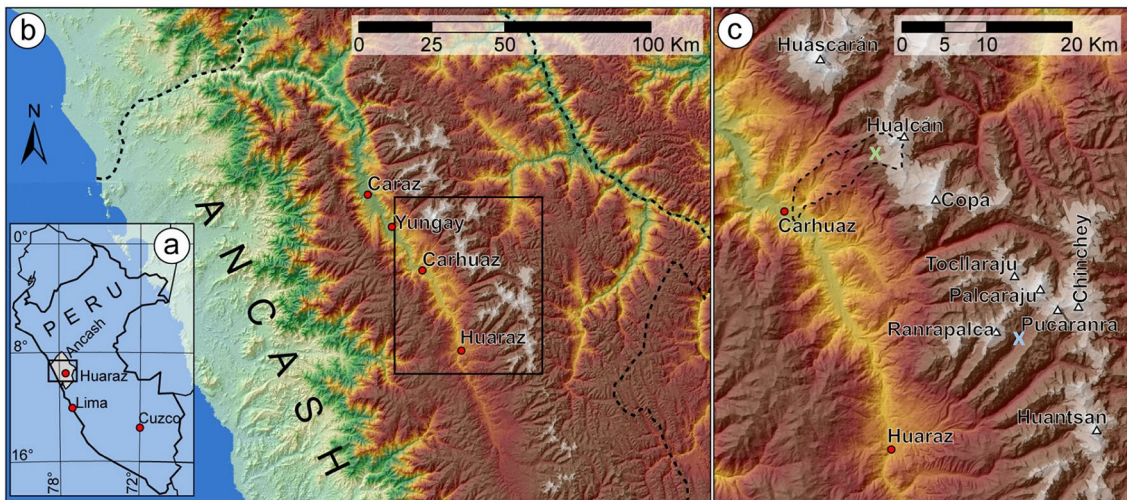


Fig. 6 a Global map of Peru. b Location of the city of Carhuaz and the city of Huaraz. c Lake 513 (green cross) and ("Case study 1: Lake 513, Cordillera Blanca, Peru") the Lake of Palcacocha (blue cross) ("Case study 2: Palcacocha Lake, Huaraz, Peru, 1941") with their corresponding catchment (black dashed line). The original map can be found in Carey et al. (2012)

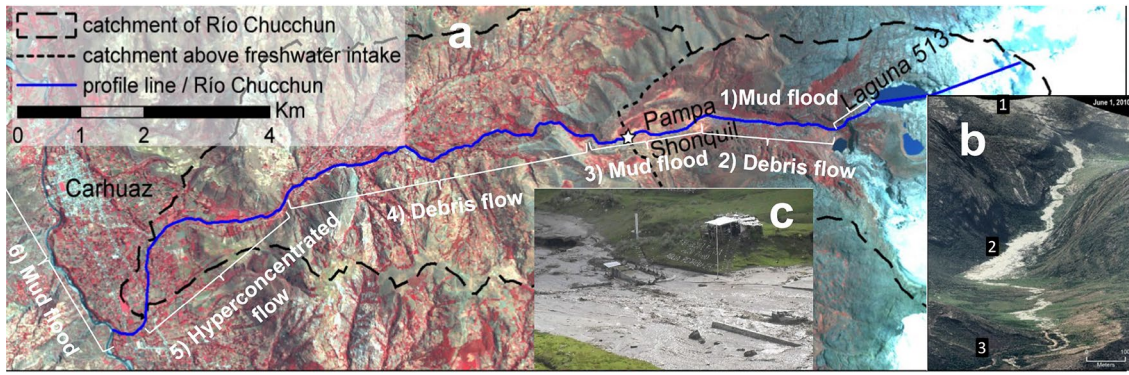


Fig. 7 **a** Map of the complete process chain of the 2010 GLOF at Lake 513. Six flow regime zones are defined following Carey et al. (2012) and Schneider et al. (2014). The flow alternates between mud, hyperconcentrated, and debris flows. A flow transition or phase separation occurs between each zone, leading to different flow regimes. The description of the flow in each zone, as well as the flow transitions, are listed in Table 2. **b** The inset depicts zones one, two, and three. We observe the deposition of solid material in zone two (Carey et al. 2012). **c** Picture taken at the star location (Pampa Shonquill) during the 2010 event of Lake 513. The flow is almost entirely fluid, corresponding to a mud flow (Photo taken by Luis Meza (Schneider et al. 2014))

$$\vec{\tau}_2 = \frac{\rho_f g \|\vec{v}_2\|^2}{\xi_f} \hat{e}_2 \quad \text{Second layer} \quad (13)$$

where $\hat{e}_i = \frac{\vec{v}_i}{\|\vec{v}_i\|}$ is a unit vector pointing in the direction of the i -th layer. For more details concerning the two-phase rheological model, we refer the reader to Meyrat (2007).

The evolving flow rheology is a fundamental aspect of the model. Friction is described as a process, depending on erosion and the immediate terrain. Indeed, it can switch from a mud flow rheology, governed almost entirely by the turbulent term, to a rocky configuration, for which the Coulomb friction term is predominant. This fact will be of major importance when simulating complex GLOF events, because the flow composition, and therefore the flow rheology, does not change only from front to tail, as for standard debris flow, but can also endure important temporal transitions from muddy flow

to a granular debris flow composition, when the flood has entrained enough solid material. Conversely, in the run-out zone, the core stops, and the fluid is washed-out, which corresponds to a transition from a debris flow to a muddy flow. Therefore, the rheology changes significantly during a single event, and a model which cannot take this evolution into account will likely not be able to give accurate numerical results with a simple set of frictional parameters. This will be demonstrated in the following case studies.

Case studies

We apply a single set of rheological parameters to model all three separate case studies. The parameters are $\mu_s = 0.16$, $\xi_s = 200 \text{ m/s}^2$, and $\xi_f = 600 \text{ m/s}^2$. A fourth parameter, the Coulomb friction of the fluid phase, is always set to zero, $\mu_f = 0$. These parameters are in close agreement to the values derived from debris flow measurements in

Table 2 Description of the Lake 513 GLOF event. Due to the long and complex valley topography, the flow exhibits five flow transitions/phase separations

Zone	Flow type	erosion	Description
1	Mud flow	Yes	Initiation as a nearly pure water surge, the solid concentration increases due to entrainment along the steep slope downstream of the lake.
2	Debris flow	Yes	The flow continues to entrain material, reaching a debris flow type. As the slope flattens, the solid matrix deposits, while the fluid is washed-out from the core, leading to phase separation.
3	Mud flow	Yes ^a	After the phase separation, the flow is almost entirely fluid. The slope is not steep enough in this zone to cause significant erosion.
4	Debris flow	Yes	As the slope increases, the erosion becomes more important and the flow evolves into a debris flow.
5	Hyperconcentrated flow	Yes	In some flatter and wider parts of the channel, lateral deposition of solid material occurred, leading to a lower solid concentration. The flow is closer to a hyperconcentrated flow.
6	Mud flow	No	The remaining part of the solid deposits in the flat valley close to Carhuaz, while the fluid continues to flow downstream.

The footnote ^a indicates lateral erosion of the bed channel

Table 3 Color code used on Figs. 8, 14, and 19. Each color corresponds to a different flow type. The flow type is computed by integrating the volumetric solid concentration over time. This classification is only used for visualization

Color	Flow type	Solid fraction Φ_s	μ_1
Blue	Water/mud flow	$0 \leq \phi_s \leq 0.2$	$0 \leq \mu_1 \leq 0.04$
Green	Hyperconcentrated flow	$0.2 < \phi_s \leq 0.6$	$0.04 < \mu_1 \leq 0.11$
Red	Debris flow/solid material deposition	$0.6 < \phi_s \leq 0.8$	$0.11 < \mu_1 \leq 0.2$

Switzerland (see Meyrat (2007)). All of the other model parameters can be found in Annex. Except for one erosion parameter (the critical shear stress), all parameters are equal in the three different simulations. Once the initial conditions are fixed, the evolution of the flow friction (entirely defined by the value of μ and ξ in our model) will be computed according to the flow composition which itself is governed by the erosion and deposition processes.

To simulate these GLOF events, we define a flow hydrograph in which the total volume of the discharge is selected to match the field observations (Somos-Valenzuela et al. 2016; Frey et al. 2018a; Carey et al. 2012; Schneider et al. 2014; Zaginaev et al. 2019a). The initial material released during the breaching process is almost completely fluid (we assume 95% fluid, 5% solid). The input hydrograph parameters are provided in Table 1. The values of the total released volume (V_{tot}), the maximum peak discharge (Q_{max}), and the time associated with the maximum peak discharge (t_{max}) are based on previous

studies (Zaginaev et al. 2019a; Mergili et al. 2020; Carey et al. 2012). The input hydrograph is defined by three points defining the discharge at a specific time (e.g., $P_1 = (0, 0)$, $P_2 = (t_{max}, Q_{max})$, and $P_3 = (t_{end}, 0)$; see Fig. 5). We linearly interpolate the discharge, $Q(t)$, between the time points (see Fig. 5). The discharge function is as follows:

$$Q(t) = \begin{cases} \frac{Q_{max}}{t_{max}} t, & \text{if } t \in [0, t_{max}] \\ \frac{Q_{max}}{t_{end}-t_{max}} (t_{end} - t), & \text{if } t \in [t_{max}, t_{end}] \end{cases} \quad (14)$$

The total release volume (V_{tot}) is defined by the integration of the discharge with respect to time, which is, using Eq. 14:

$$V_{tot} = \int_0^{t_{end}} Q(t) dt = \frac{Q_{max} t_{end}}{2}. \quad (15)$$

These equations allow the computation of t_{end} from the value of V_{tot} and Q_{max} . The peak discharge of the Aksay event is lower than the two others because we assume a sub-glacial breaching process and not a wave that overtops the moraine dam or a moraine dam failure.

All the events have been simulated using a 10 m x 10 m DEM. The dataset used for the Aksay Valley DEM is JAXA/METI ALOS PAL-SAR L1.0 2007, accessed through ASF DAAC 25 June 2022. For Lake 513, we resampled an 8 m resolution DEM derived from Spring 2012 WorldView satellite imagery. For Lake Palcacocha, we resampled a 5 m photogrammetric DEM from 2013, provided by the Peruvian Ministry of the Environment (MINAM). To simulate the 1941 Lake Palcacocha event, we did not modify the 2013 DEM to account for terrain conditions in 1941, as for example in Mergili et al. (2020). Although the channel clearly wandered between 1941 and 2013, we ran the simulations assuming the slope inclinations of the channel were approximately the same and did not vary between 1941 and 2013.

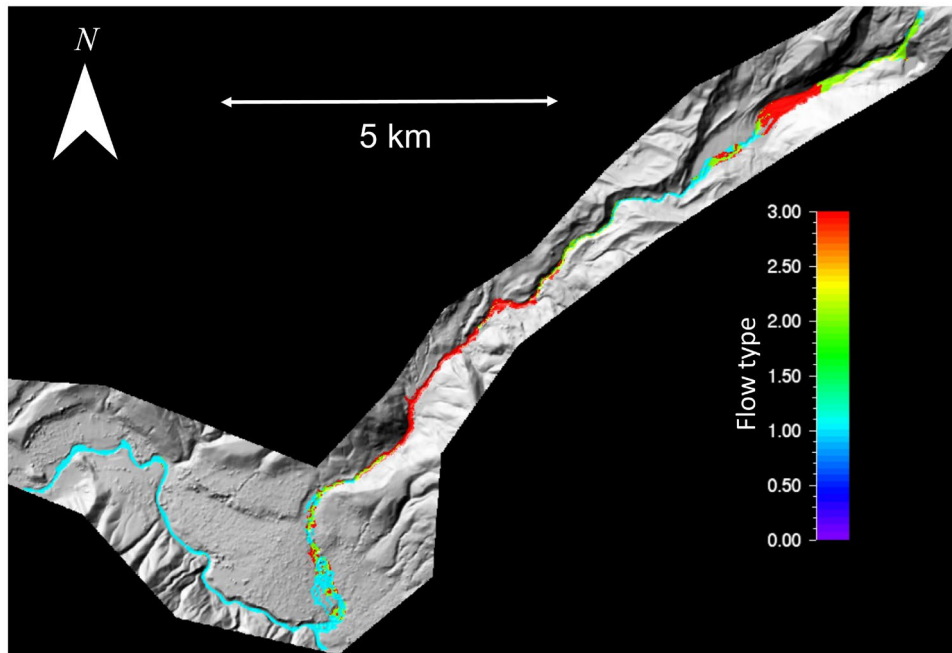


Fig. 8 Reconstruction of the flow type evolution for the event of Lake 513 in 2010. The colors represent different flow types (see Table 3). The computation is based on the volumetric solid fraction integrated over time, shown in Fig. 9. The flow transitions and phase separations, governed by entrainment and deposition processes, are captured by the model (see Table 2 and Fig. 7)

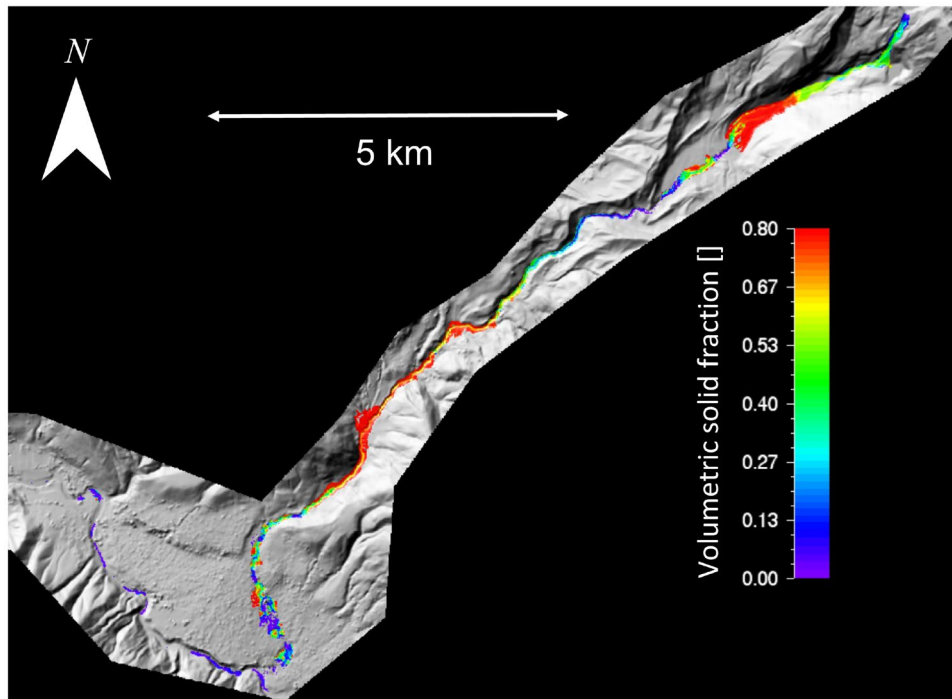


Fig. 9 Volumetric solid fraction integrated over time of the Lake 513 event of 2010. Flow type (see Table 2 and Fig. 8) is computed from the volumetric solid content

Case study 1: Lake 513, Cordillera Blanca, Peru

Lake 513 (4428 m a.s.l) is located in the Cordillera Blanca, Peru (Fig. 6). The lake is surrounded by imposing glaciers and high

mountains (peaks higher than 6000 m a.s.l. are denoted by a triangle; see Fig. 6). Lake 513 is located in the upper part of the 20 km long Chucchun catchment, which extends down to the city of Carhuaz (2640 m a.s.l.), where the Chucchun River joins the main

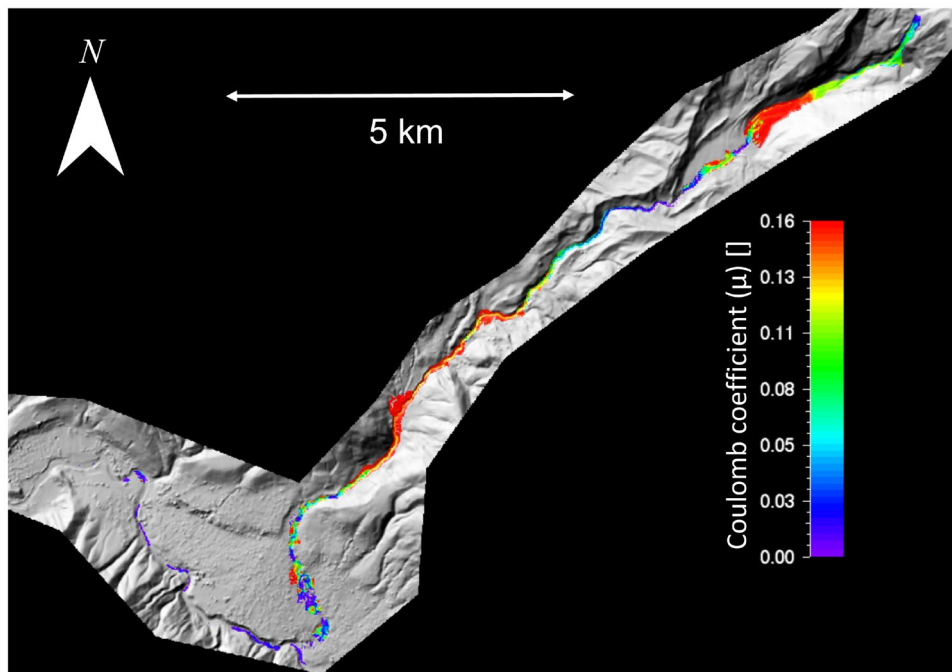


Fig. 10 Value of the Coulomb coefficient, μ , based on the flow composition and Eq. 10. The evolution of rheology is of primary importance to simulate complex events with multiple flow regimes

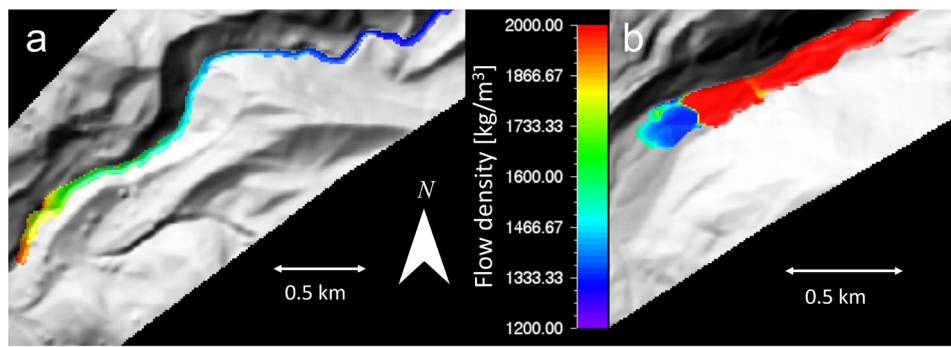


Fig. 11 **a** Flow density (for $t = 940s$) in zone four. The density is high in the front and decreases toward the tail to reach the muddy fluid density, as expected for a standard debris flow. The model is able to compute the correct flow composition (or density) in time, as well as over the length of the torrent. **b** Representation of the phase separation occurring between regions two and three. The core of the flow is stopped (red region), while the fluid is washed out (blue region)

Santa River. The valley exhibits a complex topography, with many step-like changes in elevation, slope angle, and channel width. On 11 April 2010, a 450,000 m³ rock-ice avalanche detached from the bedrock beneath the steep hanging glaciers of Mount Hualcan. The avalanche impacted the glacial lake and triggered a 24 m high displacement wave that overtopped the rock dam of the lake with a 19 m freeboard by 5 m. The event triggered a GLOF that caused severe damage to bridges, houses, roads, and agricultural land as far down as the city of Carhuaz (see Fig. 6 and Table 2). The alternation between steep and flat terrain induces flow regime transitions and phase separations, due to the deposition of solid material on the flatter track segments (Fig. 7 and Table 2). The event of 2010 is of particular interest because different flow regimes have been characterized by field work performed immediately after the event

(Carey et al. 2012; Schneider et al. 2014). The main features of the flow evolution are described in Table 2 and depicted in Fig. 7.

The flow types are computed by the model according to the definition supplied in Table 3 (see Fig. 8). The blue color corresponds to a water/muddy flow, the yellow to a hyperconcentrated flow, and the red to a debris flow (see Table 3). Only zone five, i.e., corresponding to an hyperconcentrated flow, is not well reproduced by the model. In this region, the solid material is deposited at the beginning of zone 5. Deposition in this area agrees with field observations; however, part of the solid material continued to flow until the flat valley above the city of Carhuaz. In our simulation, the part of the material flowing down the lower valley appears to be underestimated. Indeed, it is possible that fluvial bedload transport, which is not included in our model, may have transported some of this coarse sediment downstream.

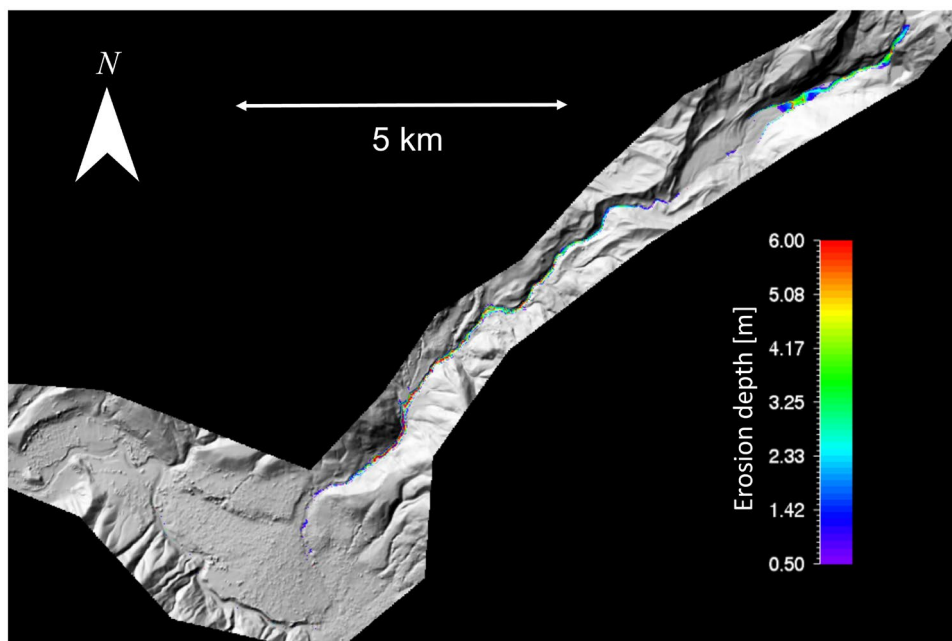


Fig. 12 Erosion depth of the Lake 513 event of 2010

Figure 9 depicts the solid volumetric concentration integrated over time. The flow types, represented in Fig. 8, are based on these results. In zones four and five, the yellow ($\phi_s \approx 0.65$) sections correspond to the flowing material, whereas the red zones ($\phi_s \approx 0.8$) located on the outer flow boundaries correspond to the deposition of solid material on the sides of the channel, which is consistent with Vilímek et al. (2015). The red part in the bottom valley (zone 5, in Fig. 9) also represents solid material deposition, as described in Carey et al. (2012) and Vilímek et al. (2015).

In Fig. 10, the calculated values of μ are depicted. Values of μ are computed from the solid volumetric concentration (Fig. 9) using Eq. 10. The average value of the calculated μ coincides for each flow type with the values found in Fig. 3. This result indicates that it is possible to model completely different flow regimes with a single set of parameters describing a process controlled change in flow rheology.

Figure 11a shows the spatial evolution of the debris flow density in region four. The front of a standard debris flow is mainly composed of large blocks and is therefore associated with a high solid concentration. Towards the end of the flow in the upstream direction, the fluid concentration increases to reach an almost mud

flow at the flow tail. Moreover, the largest density values are in the front and decrease towards the tail, as shown in Fig. 11a. The model appears to accurately compute the average solid–fluid concentration in time as well as over space.

Finally, Fig. 11b depicts the simulated phase separation between zones two and three. The core of the flow (red) is in the process of decelerating and stopping, compared with Fig. 7c, while the fluid (blue) is washed-out and can continue to flow downstream, triggering a new debris flow farther down the valley.

The mass balance of this event, including specific erosion areas, was well characterized by Vilímek et al. (2015). The erosion depth obtained by our model is depicted in Fig. 12. According to Vilímek et al. (2015), lateral erosion was observed in zone 3 but was not completely captured by the model. This may be due to the fact that in a depth-averaged model, which divides the flow into slope-perpendicular normal and slope-parallel shear stresses, might underestimate the total basal stress at steep, lateral edges. However, the strong erosion processes that occurred in regions 1, 2, 4, and 5 coincide with the model results. The authors also noted deposition in zones 4 and 5, which also could be modeled (Fig. 9).

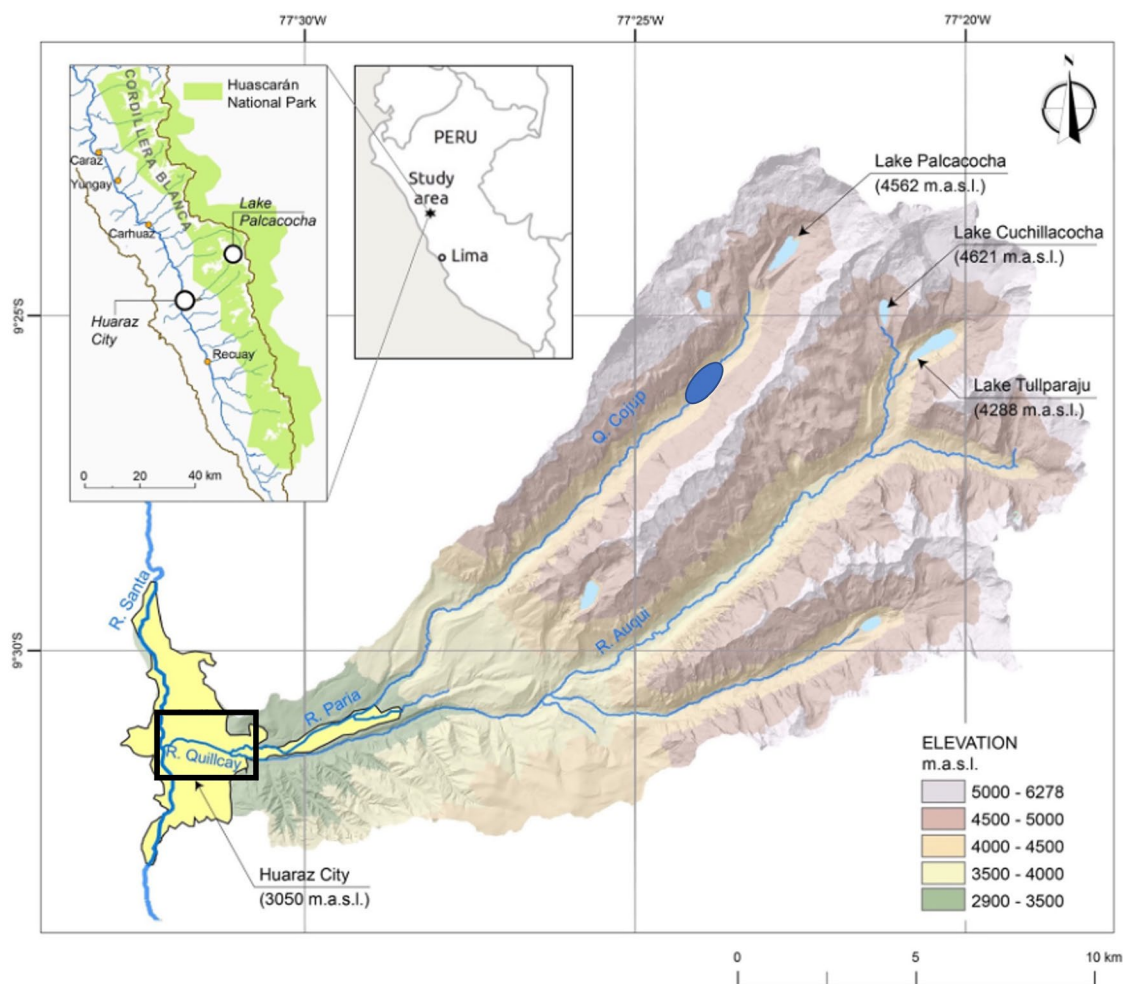


Fig. 13 Map of the Huaraz region with the Lake Palcacocha, which initiate the GLOF of 1941, including the location of Lake Jircacocha in the Cojup valley (blue ellipse). This lake was completely entrained by the event of 1941. The black rectangle shows the extent of Fig. 15. Figure modified from Frey et al. (2018b), based on Somos-Valenzuela et al. (2016)

Table 4 Description of the Lake Palcacocha GLOF event, which occurred in 1941, destroying the center of the city of Huaraz and killing 1800 persons. A more detailed description of this event can be found in Somos-Valenzuela et al. (2016); Mergili et al. (2020)

Zone	Flow type	Erosion	Description
1	Mud flow	No	Initiation as a nearly pure water surge, the small amount of solid material entrained in the moraine and below the lake stops a few hundred meters below the lake. At an elevation of \approx of 4130 m a.s.l., the Lake Jircacocha was completely entrained by the flow
2	Hyperconcentrated to debris flow	Yes	The flow starts to entrain a significant amount of solid material, increasing the solid concentration. As the flow becomes flat before and inside the city, the solid content deposits, while the fluid is washed-out from the core, leading to a phase separation
3	Mud flow	No	After the phase separation, the flow is almost entirely fluid. The slope is not steep enough in this zone to cause significant erosion processes

In Vilímek et al. (2015), the valley was divided into twelve different regions. For our study, we used only. The results of Vilímek et al. (2015) have been averaged to fit our zone definition.

In this case study, the overall mass balance of the event as well as the solid deposition behavior are accurately reproduced indicating that the erosion behavior integrated over the entire length of the torrent appears to be reasonable. However, there can be regions where the simulated erosion is over or underestimated. Finally, we underscore the fact that with a model that cannot reproduce the solid–fluid internal composition of such a flow, the rheology has to be tuned by hand in order to obtain correct results. Indeed, in the case of the back-computation of Lake 513 with the one-phase

RAMMS model (Carey et al. 2012), five different set of frictional coefficients have to be used to reproduce it accurately. This induces significant uncertainties about the numerical results and cannot be done without past information on the back-computed event.

Case study 2: Palcacocha Lake, Huaraz, Peru, 1941

Lake Palcacocha (4562 m a.s.l.) is located in the Cordillera Blanca, above Huaraz (3050 m a.s.l.), in Peru (Fig. 13). Similar to the Lake 513 case study, the lake is surrounded by high mountains and large hanging glaciers. The lake drains into the Cojup river, which

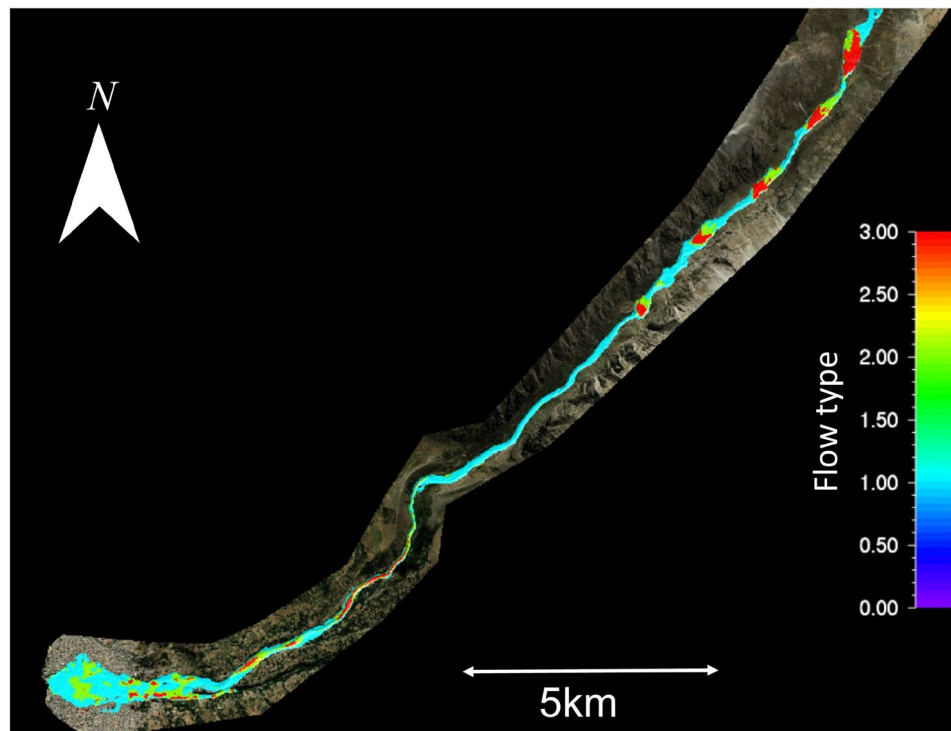


Fig. 14 Different flow types (see Table 3) that occurred during the Lake Palcacocha event. The simulated flow behavior corresponds to the observations (Table 4). The red line represents the separation between zones one and two. The flow has a high fluid concentration compared to the other two case studies (Figs. 8 and 19). The high fluid concentration is due to the entrainment of the glacier lake while flowing in the Cojup valley

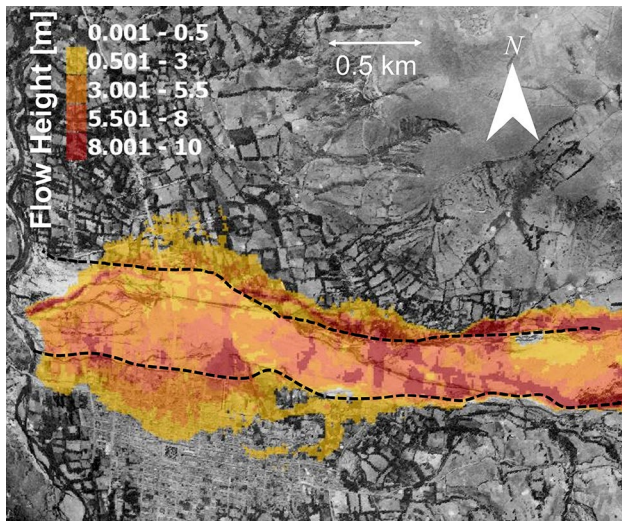


Fig. 15 Comparison between the observed debris flow fan of the 1941 event (background picture) and maximum flow height computed by the model. The black dashed line represents the observed deposit zone. The heights lower than 50 cm are not depicted. The background picture is from A. Cicoira

arrives directly on the east side of Huaraz, after approximately 20 km (Fig. 13). In 1941, a breach formed in the moraine dam of Lake Palcacocha, possibly triggered by the impact of a mass movement (Mergili et al. 2020). The GLOF flowed downstream the Cojup

valley. After completely entraining another lake (Lake Jircacocha), which does not exist anymore (Vilímek et al. 2005; Emmer and Vilímek 2014; Wegner et al. 2014) (see Fig. 13), the resulting debris flow reached and destroyed a large part of the city of Huaraz killing approximately 1800 persons Wegner et al. (2014). The damage to buildings and agricultural infrastructure, located either in the city of Huaraz, and also further downstream, was immense (Carey 2010; Evans et al. 2009).

Several numerical studies have already been performed of this event to back-calculate the 1941 outburst Mergili et al. (2020) and to predict future GLOF events (Somos-Valenzuela et al. 2016; Frey et al. 2018b). These studies indicate that the flow started as a water surge. The material entrained in the glacier moraine and on the steep slopes just below the initiation were deposited at the beginning of the long and flat Cojup valley. Up to an elevation of 4000 m a.s.l. (zone one in Fig. 14 and in Table 4), no surface erosion was observed, indicating a flow with a low solid concentration. Before the 1941 event, a lake was present in the valley at an elevation of approximately 4130 m a.s.l. (see Fig. 13), which was completely entrained by the flow. At an elevation of around 4000 m a.s.l. (limit between zones one and two Fig. 14), the slope increases and significant erosion starts, leading to an increase in the solid concentration. The core stopped on flatter terrain before and inside Huaraz. Detailed studies by the Instituto Nacional de Defensa Civil have been performed to quantify the deposit area in the city. In Fig. 15, we compare the observed deposit with the model outputs. The deposit area is slightly larger than the real one; however, we underline that the simulation is done without any

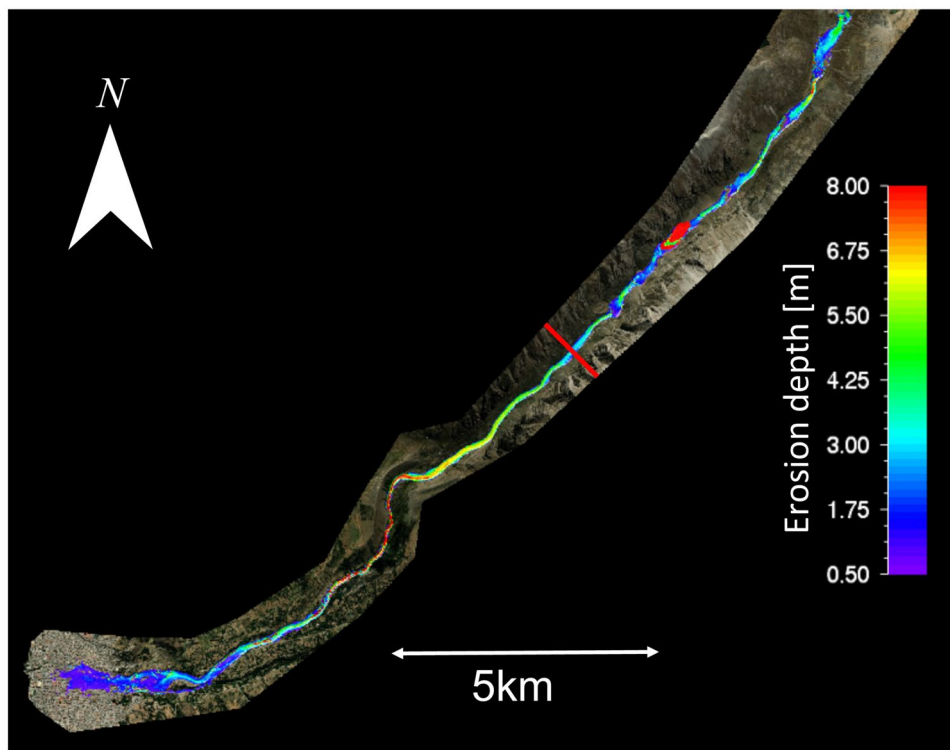


Fig. 16 Erosion depth obtained with the two-layer model. The red line represents the beginning of the area where significant erosion processes have been observed in the field (Frey et al. 2018a). The red part before the red line (zone 1) represents the entrainment of the Lake Jircacocha (see Fig. 13)

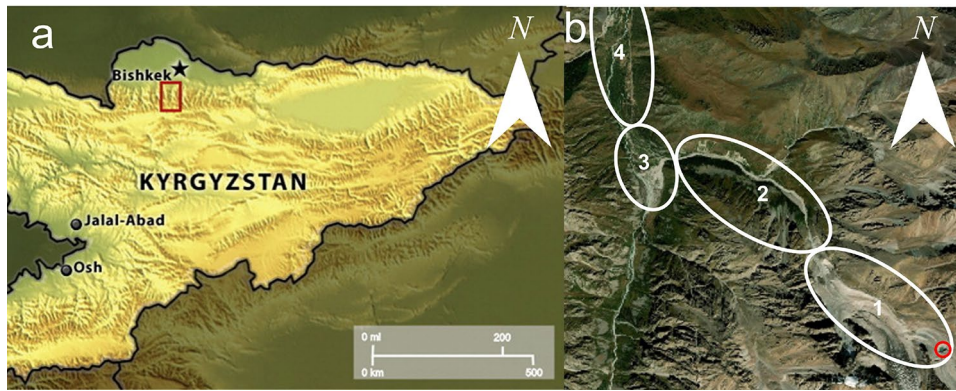


Fig. 17 **a** Location of the Ala-Archa Valley (National Park) in Northern Tien Shan. **b** Orthophoto of the Aksay valley. The glacier lake is indicated in red, while the valley itself has been decomposed into three different regions. The first one (1) with a low slope angle, the step channel (2), the run-out debris flow zone (3), and finally the gentle valley (4) which flows downwards the plain. Each zone exhibits different types of flow behavior, and flowing transition occurs between them. However, no field observations concerning the flow types are available

adaptation of the model free parameters. For example, in Mergili et al. (2020), the simulation is performed by adapting the model parameters as the Coulomb coefficient μ (called frictional angle δ in Mergili et al. (2020)). After the stopping and deposition of the solid material, the flow, which was mainly composed of fluid with fine suspended sediments, continued to flow downstream the valley and cause great damage. This lower region was not simulated due to the unavailability of an accurate DEM, as well as due to the fact that the flow did not transition into another flow region. Therefore, we define only two flow regime zones for this case, which are separated by a red line in the plots.

Figure 16 depicts the erosion depth obtained for the simulation of the 1941 event. Simulation results found in Frey et al. (2018a) indicate that erosion occurred mainly a few hundred meters downstream the lake and in the lower part of the valley (see Table 4). This region is steeper than zone two, shown

in Fig. 16. In between these two regions, no significant evidence of erosion was observed. The model captures this behavior, where the erosion is much stronger just below the release and in zone two. The red polygon in the Cojup valley corresponds to the entrainment of the Lake Jircacocha present before the 1941 event. The surface and depth of the lake have been calibrated to fit the lake volume, i.e., $3.3 \times 10^6 \text{ m}^3$ (Mergili et al. 2020). In this specific zone, the density of the entrained sediment is set to be the same as the fluid density, and stronger erosion is considered. The lake's entrainment does not only change the mass balance of the flow but its entire dynamics due to the fluidization of the flow. Indeed, the correct debris flow run-out distance (Fig. 15) would be impossible to model without the entrainment of the lake. Indeed, without the entrainment of the Lake Jircacocha, the solid materials composing the debris flow would deposit before the city of Huaraz.

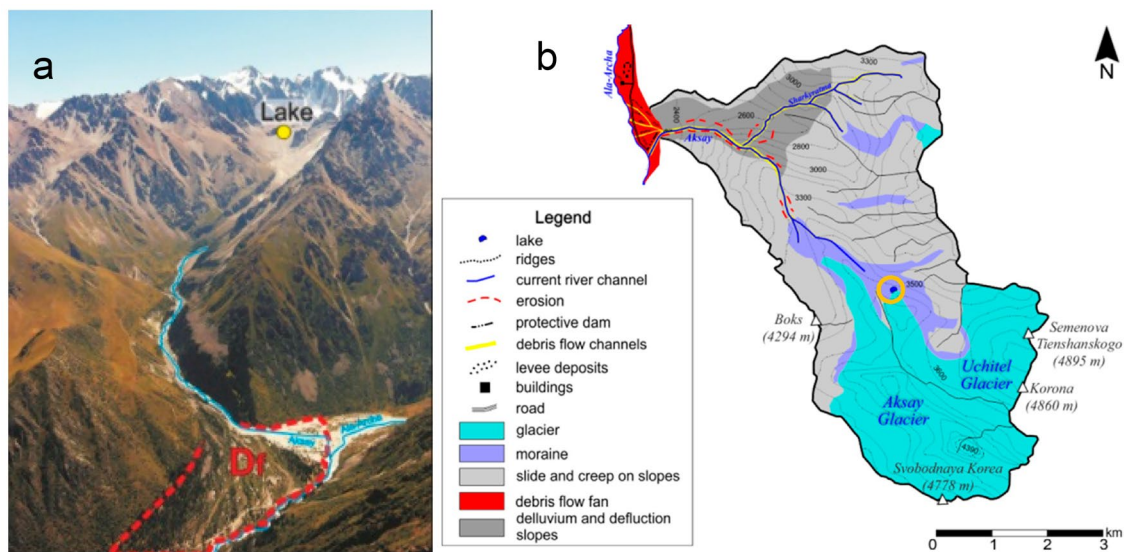


Fig. 18 **a** Debris flow fan zone. The red dotted line is the deposit zone delineated according to field observations (Zaginaev et al. 2019a). **b** Map of the Aksay Valley. The erosion area is denoted by the red dotted line, while the initiating lake is marked by an orange circle. Credit for the map: Zaginaev et al. (2019a)

Table 5 Description of the Aksay valley GLOF event

Zone	Flow type	Erosion	Description
1	Mud flow to hyperconcentrated flow	no	Initiation as a nearly pure water surge, the solid concentration remains low because no significant erosion occurs
2	Debris flow	yes	The flow starts to entrain material, and the volumetric solid concentration increases
3	Debris flow (deposition)	no data	As the flow reaches flatter terrain, a phase separation occurs
4	mud flow	no	After the phase separation, the flow is almost entirely fluid

Case study 3: Aksay Valley, Ala-Archa National Park, Kyrgyzstan

The Ala-Archa National park is located along the Kyrgyz Ridge, 40 km south of Bishkek, Kyrgyzstan (Fig. 17a). The debris flow fan of Aksay Valley is the largest in the Ala-Archa National Park, and several studies concerning debris flow monitoring, analysis, and simulation have been performed in this specific torrent (Zaginaev et al. 2016, 2019a, b). The valley's elevation varies from 4895 m a.s.l to 2200 m a.s.l (run-out on the fan). Two glaciers can be found in the catchment's upper part: the Aksay glacier and the Uchitel Glacier (Fig. 17b). At the receding end of the Uchitel glacier stands a lake, which is the primary source of the GLOFs in this valley. The valley below the lake can be decomposed into three distinct areas. The first one (denoted (1) on Fig. 17c) is a 2.3 km section

characterized by a low average slope angle (less than 10°). It is followed by a 4.0 km long steeper section (denoted (2) on Fig. 17c) with a slope angle around 15° which ends in the bottom valley, i.e., the run-out area ((3) on Fig. 17c). This run-out section is almost flat (less than 5°).

As we assume that the GLOF initiates with the outburst of the glacier lake, we expect a flood-type flow in the upper region (zone 1, Fig. 17c). Indeed, in this region, no significant erosion was observed. In zone 2, erosion processes started to become stronger; see Fig. 18b. As a consequence, we expect a flow with a higher solid concentration. Finally, the core of the debris flow stopped in the Aksay valley (see Fig. 18a and Zaginaev et al. (2019b)) (zone 3), and the fluid continued to flow downstream the valley (zone 4), almost without erosion processes. The flow history is summarized in Table 5.

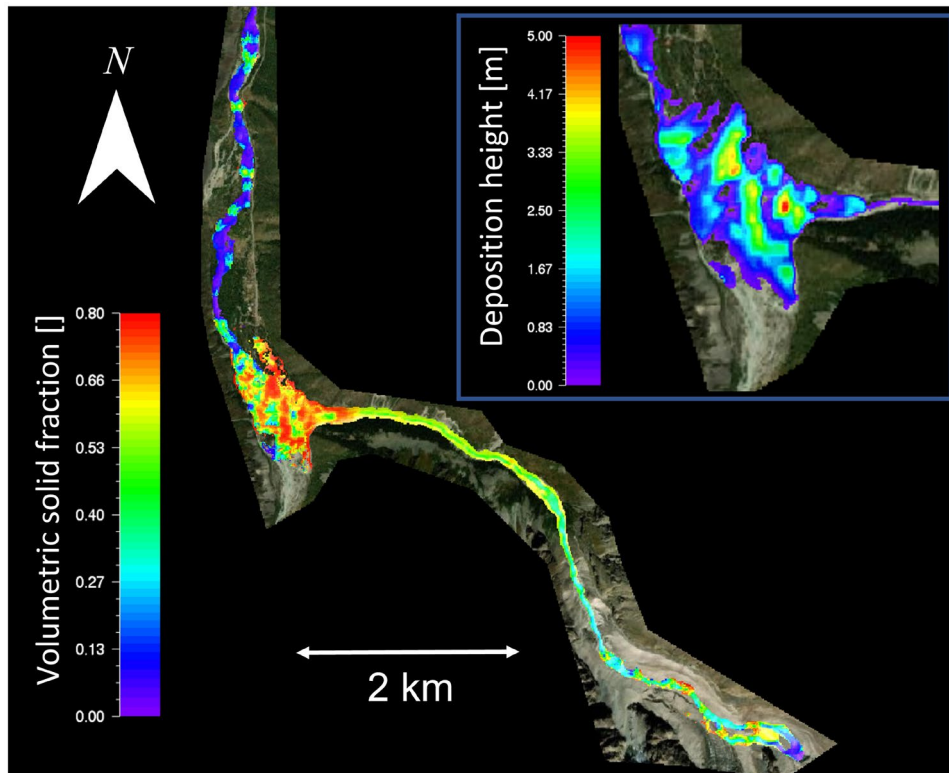


Fig. 19 Solid volumetric fraction of the flow, integrated over time. As expected, the flow is in a low solid concentration configuration in the first zone, where no erosion was observed. In the steeper part (zone 2), the volumetric solid concentration increases due to the erosion of solid material. Finally, the core deposits (zone 3) and the fluid is washed out and continue to flow downward (zone 4). The sub-figure on the upper right corner is the solid deposit of the flow, which is in good agreement with field observation reported in Fig. 18a

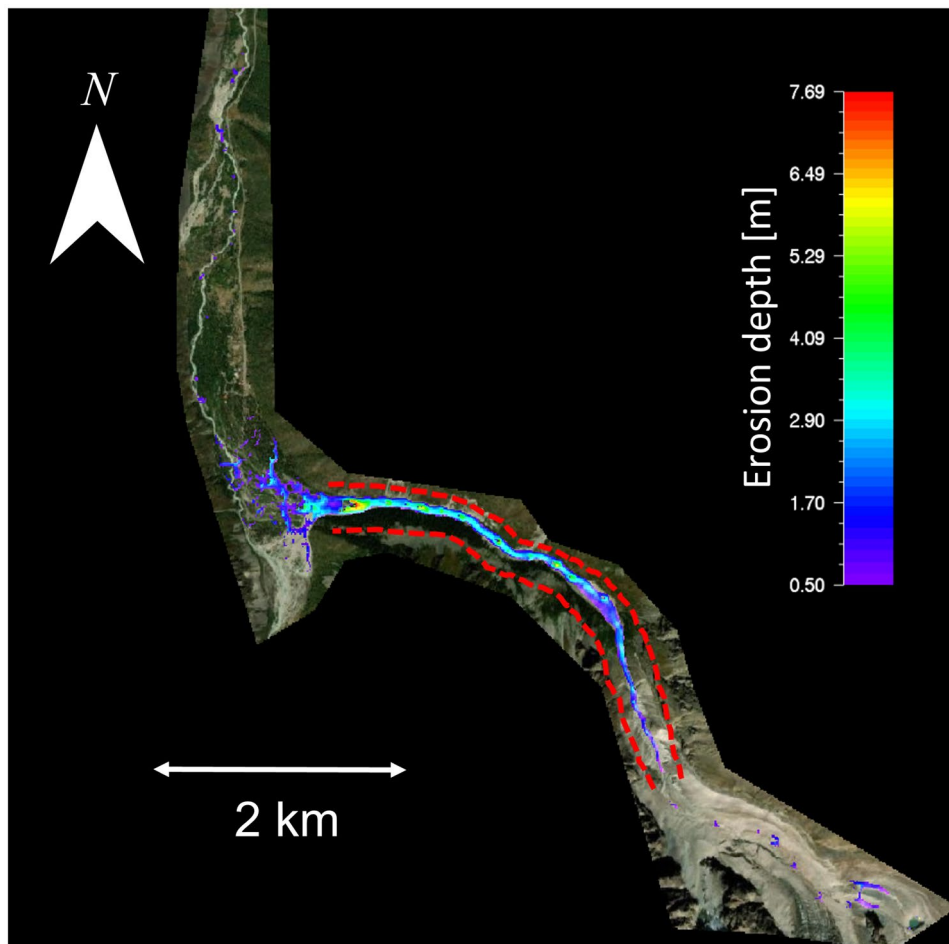


Fig. 20 Erosion depth obtained with the two-layer model. The red dotted line is the approximately observed erosion, shown in Fig. 18b, computed after field observations

Figure 19 shows the solid volumetric concentration integrated over time. One can see that the general behavior detailed above, i.e., flow transition from zone 1 to 2 and phase separation in zone 3, is captured by the model. Following Zaginaev et al. (2019a, b), we can estimate the run-out zone distance for the debris flow event of 1960 using satellite imagery, see Fig. 18a. The average run-out area of the previous monitored event is approximately $A_{\text{run-out}} \approx 0.2 \text{ km}^2$ (Zaginaev et al. 2019b). In our simulation, we have the same order of magnitude for the value of the deposition area. The discharge could have been adjusted to fit the disposition area perfectly; however, without precise information about the peak discharge, we did not do so. Further, the run-out area detailed on Fig. 18a, is similar to the one we obtain in Fig. 19.

In Zaginaev et al. (2019a), detailed observations of the erosion areas are provided (see Fig. 18b). Figure 20 depicts the numerically obtained spatial distribution of the erosion. The erosion depth is difficult to discuss due to a lack of information. However, the model accurately reproduces the erosion pattern (the region with or without erosion).

Discussion and conclusions

GLOFs exhibit complex flow regime transitions due to the continually changing solid–fluid composition of the flow. Small inclination changes in the valley profile, or enlargement of the channel width, can produce solid–fluid phase separations, initiating the deposition of solid material. As GLOFs, by definition, initiate from a lake outburst, the initial flow is mainly fluid, leading to a mud flow. However, with the mobilization of loose sediments from the bed and channel sides, the floods acquire solid material, which leads to a transition from a mud flow to a hyperconcentrated flow. With the entrainment of more solid debris, the flows evolve to viscous, granular-type debris flows. These types of flow transitions could be captured by applying a Voellmy-type flow rheology (Meyrat 2007) within the framework of a two-layer debris flow model (Meyrat et al. 2022). The evolution of the internal solid–fluid composition governs the flowing properties, including the steady-state velocity in the channel or the run-out distance on flatter terrain. We apply a model to simulate the different flow regimes observed in the three case

studies (Figs. 8, 14, and 19). The Lake 513 event is of great interest because it exhibits different flow regimes due to the long flowing distance (around 20 km) over complex terrain topography. The field observations performed after the event (Carey et al. 2012, Schneider et al. 2014) permit a classification of the succession of flow types that enabled the validation of our model, which reproduces the events accurately from after the outburst to deposition. The erosion pattern and deposition area, described in Vilímek et al. (2015), are also captured by the model. Although the model predicts with reasonable accuracy the erosion patterns, the run-out distances, the solid deposits, and affected areas of the other two events (Figs. 15, 16, 19, and 20), the evaluation of model performance is more uncertain. The exact erosion depths are not known precisely, but the regions with and without erosion are well documented. These results indicate that both the erosion patterns and run-out distances can be captured by the model, which is an indirect validation of the model rheology.

The ability to model this complex flow behavior has three main origins.

1. Firstly, a full *two-component approach* is used to predict the velocity of the solid debris with bonded fluid or the free (muddy) fluid. The physical and mathematical construction of the model is built on the foundation of a two-fluid, two-layer model involving well-constrained mass exchanges between the two fluid components. Unlike other models (Bouchut et al. 2016; Pitman and Le 2005; Iverson and George 2014; George and Iverson 2014), the fluid velocity is not computed using a Darcy-like approximation, which reduces two-component models to the solution of a single phase.
2. Secondly, embedded into the governing equations is a *theory of granular dilatancy*. Mathematically, this requires the solution of an additional differential equation describing the production and decay of granular fluctuation energy, which drives the dispersive actions in the solid mixture. Although computationally more intensive, this approach enables us to predict the separation of the solid and fluid phases. The mass and momentum exchanges induced by the dilation of the solid matrix play a role in the interactions between the solid and the fluid components. It also controls the collapse of the solid matrix on flatter slope inclinations, allowing for phase separation and de-watering.
3. Finally, the central aspect of the model is the *evolving rheology*. A uniform and constant rheology fails to reproduce the dynamics of complex events such as GLOFs (Westoby et al. 2014) even if they can be applied with significant tuning to model specific debris flow events. For example, five different zones associated with different rheology coefficients (μ and ξ) had to be defined to reproduce the event of the Lake 513 (Carey et al. 2012) when using the one-phase, constant rheology RAMMS model. The use of Eq. 10 allows the two-layer model to reproduce a fluid-like behavior, driven by the turbulent friction, but also a granular-like flow, driven by the Coulomb friction, within a single mathematical framework. In this model, we assume a simple relation between the flow composition, given by ϕ_s and ϕ_f , and the rheology, represented by $\mu(\phi_s)$ and $\xi(\phi_s)$. More accurate data would be needed to develop a more sophisticated mathematical

model. Preliminary laboratory studies show that in the range of $0.3 < \phi_s < 0.9$, the shearing intensity and the volumetric fluid concentration can be approximated by a linear relation.

The dependency of the rheological parameters on the flow composition also allows us to reduce the interval of possible values for the frictional parameters, μ_s , ξ_s , and ξ_f . Indeed, the same set value was used for the three scenarios, which exhibit different behaviors and a wide variation of flow volumes, i.e., 35,000 m³ for the event of Aksay valley and 10,000,000 m³ for the Lake Palcacocha event (without entrainment). The uniformity of the rheological free parameters is one of the attractive features of the model and will be of primary importance when applying it to hazard analysis prediction. Indeed, a model which is not able to reproduce the flow transitions and phase separations would have to be tuned to perform relevant simulations. This implies a major limitation for *a priori*-type applications, when there is no historical information available. Confidence in the free parameters is a central question in numerical models. A debris flow model should be able to perform accurate simulations of real events using the lowest number of free parameters possible. Back-calculation of existing events with models that contain few parameters is a first step to developing powerful, predictive tools for practical applications. We applied the same frictional parameters within the framework of a theory based on modeling flow dilations within the solid matrix. Modeling flow behavior in this way produced a model with only one free parameter. This is the ratio between α , representing the production of solid dilations, and β , representing its decay. We fixed the production α ; hence, β is the free parameter governing flow regime transitions. Interestingly, we were able to use the same value of β for all three events. More case studies are clearly required to determine if this approach is valid in general.

The uniformity of the rheological parameters was also helpful to better model erosion processes. In the three case studies, the critical shear coefficient had to be adapted to correctly simulate the Palcacocha 1941 event. Even if the release material, as well as the terrain topography, are generally known with reasonable accuracy, the bed properties of the entire torrent are largely unknown. Therefore, the adaptation of the erosion parameters is rather linked to a need for more accurate knowledge about precise boundary conditions rather than a specific model deficiency. It is to be expected that the erosion parameters must be selected for a specific site. The selection of parameters remains a modeling problem that is, in the end, a more general problem well-known to the debris flow engineering community.

Acknowledgements

The authors acknowledge the support of the CCAMM (Climate Change and Alpine Mass Movements) research initiative of the Swiss Federal Institute for Forest, Snow, and Landscape Research. We are especially thankful for the support of Dr. A. Bast program coordinator. We acknowledge the GLOFCA project for funding (A. Cicoira and H. Frey) as well Vitalii Zaginajev for fruitful discussions about the Ala Archa study case.

Funding

Open Access funding provided by Lib4RI – Library for the Research Institutes within the ETH Domain: Eawag, Empa, PSI & WSL.

Declarations

Conflict of interest The authors declare no competing interests.

Annex

Name	Symbol	Value	Unity []
Solid density	ρ_s	2500	kg/m^3
Fluid density	ρ_f	1300	kg/m^3
Co-volume density ^{*a1}	ρ_{co}	2000	kg/m^3
Solid Coulomb coefficient	μ_s	0.16	-
Fluid Coulomb coefficient	μ_f	0.0	-
Solid turbulent coefficient	ξ_s	200	m/s^2
Fluid turbulent coefficient	ξ_f	600	m/s^2
Configurational energy production	α	0.2	-
Configurational energy decay	β	0.07	$1/s$
Steady state coefficient	$\Gamma = \frac{\alpha}{\beta}$	2.86	s
Entrained density	ρ_e	2000	kg/m^3
Solid erosion rate	E_s	0.03	m/s
Fluid erosion rate	E_f	0.003	m/s
Critical shear stress	τ_c^{*b}	0.5	kPa
Critical shear coefficient	$\frac{d\tau_c^{*b}}{dz}$	-0.2/-0.4 ^{*c}	m/kPa
Critical erosion velocity	v_c	0.5	m/s
Gridsize	Δx	10	m
Granule size	Gr	7	cm

^{*a} defined without fluid in the interstitial space in between the solid particles

^{*b} For the definitions of these values, refer to Frank et al. (2015, 2017)

^{*c} The first value corresponds to the Lake 513 and Aksay events and the second one to the Lake Palcacocha event

Open Access This article is licensed under a Creative Commons Attribution 4.0 International License, which permits use, sharing, adaptation, distribution and reproduction in any medium or format, as long as you give appropriate credit to the original author(s) and the source, provide a link to the Creative Commons licence, and indicate if changes were made. The images or other third party material in this article are included in the article's Creative Commons licence, unless indicated otherwise in a credit line to the material. If material is not included in the article's Creative Commons licence and your intended use is not permitted by statutory regulation or exceeds the permitted use, you will need to obtain permission directly from the copyright holder. To view a copy of this licence, visit <http://creativecommons.org/licenses/by/4.0/>.

References

- Badoux A, Graf C, Rhyner J, Kuntner R, McArdell BW (2009) A debris-flow alarm system for the alpine illgraben catchment: design and performance. *Nat Hazards* 49(3):517–539
- Bartelt P, McArdell B, Graf C, Christen M, Buser O (2016) Dispersive pressure, boundary jerk and configurational changes in debris flows. *Int J Eros Control Eng* 9(1):1–6
- Bindereif L (2022) Simulation of debris flows at the Ritigraben torrent, Valais, Switzerland. Master thesis
- Bouchut F, Fernández-Nieto ED, Mangeney A, Narbona-Reina G (2016) A two-phase two-layer model for fluidized granular flows with dilatancy effects. *J Fluid Mech* 801:166–221
- Bouchut F, Fernández-Nieto ED, Koné EH, Mangeney A, Narbona-Reina G (2017) A two-phase solid-fluid model for dense granular flows including dilatancy effects: comparison with submarine granular collapse experiments. In: EPJ Web of Conferences, EDP Sciences, vol 140, p 09039
- Buser O, Bartelt P (2009) Production and decay of random kinetic energy in granular snow avalanches. *J Glaciol* 55(189):3–12
- Carey M (2010) In the shadow of melting glaciers: climate change and Andean society. Oxford University Press
- Carey M, Huggel C, Bury J, Portocarrero C, Haeberli W (2012) An integrated socio-environmental framework for glacier hazard management and climate change adaptation: lessons from Lake 513, Cordillera Blanca, Peru. *Clim Change* 112(3):733–767
- Cicoira A, Blatny L, Li X, Trottet B, Gaume J (2022) Towards a predictive multi-phase model for alpine mass movements and process cascades. *Eng Geol* 310:106866
- Dunning S, Taylor C, Robinson TR (2023) Glacial lake outburst floods threaten millions globally. *Nat Commun* 14(487)
- Emmer A (2017) Glacier retreat and glacial lake outburst floods (GLOFs). In: Oxford Research Encyclopedia of Natural Hazard Science
- Emmer A, Vilímek V (2014) New method for assessing the susceptibility of glacial lakes to outburst floods in the Cordillera Blanca, Peru. *Hydrol Earth Syst Sci* 18(9):3461–3479
- Emmer A, Allen SK, Carey M, Frey H, Huggel C, Korup O, Mergili M, Sattar A, Veh G, Chen TY et al (2022) Progress and challenges in glacial lake outburst flood research (2017–2021): a research community perspective. *Nat Hazard* 22(9):3041–3061
- Evans SG, Bishop NF, Smoll LF, Murillo PV, Delaney KB, Oliver-Smith A (2009) A re-examination of the mechanism and human impact of catastrophic mass flows originating on Nevado Huascarán, Cordillera Blanca, Peru in 1962 and 1970. *Eng Geol* 108(1–2):96–118
- Farinotti D, Longuevergne L, Moholdt G, Duethmann D, Mölg T, Bolch T, Vorogushyn S, Güntner A (2015) Substantial glacier mass loss in the Tien Shan over the past 50 years. *Nat Geosci* 8(9):716–722
- Frank F, McArdell BW, Huggel C, Vieli A (2015) The importance of entrainment and bulking on debris flow runout modeling: examples from the Swiss Alps. *Nat Hazard* 15(11):2569–2583
- Frank F, McArdell BW, Oggier N, Baer P, Christen M, Vieli A (2017) Debris-flow modeling at Meretschibach and Bondasca catchments, Switzerland: sensitivity testing of field-data-based entrainment model. *Nat Hazard* 17(5):801–815
- Frey H, Huggel C, Chisolm RE, Baer P, McArdell B, Cochachin A, Portocarrero C (2018a) Multi-source glacial lake outburst flood hazard assessment and mapping for Huaraz, Cordillera Blanca, Peru. *Front Earth Sci* 6:210
- Frey H, Huggel C, Chisolm RE, Baer P, McArdell B, Cochachin A, Portocarrero C (2018b) Multi-source glacial lake outburst flood hazard assessment and mapping for Huaraz, Cordillera Blanca, Peru. *Front Earth Sci* 6:210
- Gaume J, Gast T, Teran J, Van Herwijnen A, Jiang C (2018) Dynamic anticrack propagation in snow. *Nat Commun* 9(1):3047
- Gaume J, van Herwijnen A, Gast T, Teran J, Jiang C (2019) Investigating the release and flow of snow avalanches at the slope-scale using a unified model based on the material point method. *Cold Reg Sci Technol* 168:102847
- George DL, Iverson RM (2014) A depth-averaged debris-flow model that includes the effects of evolving dilatancy. II. Numerical predictions and experimental tests. *Proceedings of the Royal Society A: Mathematical, Physical and Engineering Sciences* 470(2170):20130820
- Graf C, Christen M, McArdell BW, Bartelt P (2019) Overview of a decade of applied debris-flow runout modeling in Switzerland, An: challenges

- and recommendations. Association of Environmental and Engineering Geologists; special publication 28
- Hooke RL, Iverson NR (1995) Grain-size distribution in deforming sub-glacial tills: role of grain fracture. *Geology* 23(1):57–60
- Hungr O, Leroueil S, Picarelli L (2014) The Varnes classification of landslide types, an update. *Landslides* 11(2):167–194
- Iverson RM (2005) Debris-flow mechanics. *Debris-flow hazards and related phenomena* pp 105–134
- Iverson RM (1997) The physics of debris flows. *Rev Geophys* 35(3):245–296
- Iverson RM (2003) The debris-flow rheology myth. *Debris-flow Hazards Mitigation: Mechanics, Prediction, and Assessment* 1:303–314
- Iverson RM, Denlinger RP (2001) Flow of variably fluidized granular masses across three-dimensional terrain: 1. Coulomb mixture theory. *J Geophys Res Solid Earth* 106(B1):537–552
- Iverson RM, George DL (2014) A depth-averaged debris-flow model that includes the effects of evolving dilatancy. I. Physical basis. *Proceedings of the Royal Society A: Mathematical, Physical and Engineering Sciences* 470(2170):20130819
- Liboutry L (1977) Glaciological problems set by the control of dangerous lakes in Cordillera Blanca, Peru. II. Movement of a covered glacier embedded within a rock glacier. *J Glaciol* 18(79):255–274
- Mandli KT (2011) Finite volume methods for the multilayer shallow water equations with applications to storm surges. PhD thesis
- McArdell BW, Sartori M (2020) The Illgraben torrent system. In: *Landscapes and Landforms of Switzerland*, Springer, pp 367–378
- Medeu AR, Popov NV, Blagoveshchenskiy VP, Askarova MA, Medeu AA, Ranova SU, Kamalbekova A, Bolch T (2022) Moraine-dammed glacial lakes and threat of glacial debris flows in South-East Kazakhstan. *Earth Sci Rev* 229:103999
- Mergili M, Pudasaini SP, Emmer A, Fischer JT, Cochachin A, Frey H (2020) Reconstruction of the 1941 GLOF process chain at lake Palcacocha (Cordillera Blanca, Peru). *Hydrol Earth Syst Sci* 24(1):93–114
- Meyrat G, McArdell B, Müller CR, Munch J, Bartelt P (2007) Voellmy-type mixture rheologies for dilatant, two-layer debris flow models. *Landslides* 1(1):1–2
- Meyrat G, McArdell B, Ivanova K, Müller C, Bartelt P (2022) A dilatant, two-layer debris flow model validated by flow density measurements at the Swiss illgraben test site. *Landslides* 19(2):265–276
- Mikoš M, Bezak N (2021) Debris flow modelling using RAMMS model in the alpine environment with focus on the model parameters and main characteristics. *Front Earth Sci* 8:605061
- Petrakov D, Shpuntova A, Aleinikov A, Kääh A, Kutuzov S, Lavrentiev I, Stoffel M, Tutubalina O, Usabaliev R (2016) Accelerated glacier shrinkage in the Ak-Shyirak massif, Inner Tien Shan, during 2003–2013. *Sci Total Environ* 562:364–378
- Petrakov DA, Chernomorets SS, Viskhadzhieva KS, Dokukin MD, Savernyuk EA, Petrov MA, Erokhin SA, Tutubalina OV, Glazyrin GE, Shpuntova AM et al (2020) Putting the poorly documented 1998 GLOF disaster in Shakhimardan River valley (Alay Range, Kyrgyzstan/uzbekistan) into perspective. *Sci Total Environ* 724:138287
- Pierson TC (2005) Hyperconcentrated flow–transitional process between water flow and debris flow. In: *Debris-flow hazards and related phenomena*, Springer, pp 159–202
- Pitman EB, Le L (2005) A two-fluid model for avalanche and debris flows. *Philos Trans R Soc A Math Phys Eng Sci* 363(1832):1573–1601
- Pudasaini SP, Hutter K (2007) *Avalanche dynamics: dynamics of rapid flows of dense granular avalanches*. Springer Science & Business Media
- Pudasaini SP (2012) A general two-phase debris flow model. *J Geophys Res Earth Surf* 117(F3)
- Ramms (2017) RAMMS:DEBRISFLOW user manual. Davos, Switzerland: Eth
- Reynolds O (1885) LVII. On the dilatancy of media composed of rigid particles in contact. with experimental illustrations. *The London, Edinburgh, and Dublin Philosophical Magazine and Journal of Science* 20(127):469–481
- Richardson SD, Reynolds JM (2000) An overview of glacial hazards in the Himalayas. *Quatern Int* 65:31–47
- Savary É, Zech Y (2007) Boundary conditions in a two-layer geomorphological model. Application to a. *J Hydraul Res* 45(3):316–332
- Schlunegger F, Badoux A, McArdell BW, Wendeler C, Schnydrig D, Rieke-Zapp D, Molnar P (2009) Limits of sediment transfer in an alpine debris-flow catchment, Illgraben, Switzerland. *Quatern Sci Rev* 28(11–12):1097–1105
- Schneider D, Huggel C, Cochachin A, Guillén S, García J (2014) Mapping hazards from glacier lake outburst floods based on modelling of process cascades at Lake 513, Carhuaz, Peru. *Adv Geosci* 35:145–155
- Shugar DH, Burr A, Haritashya UK, Kargel JS, Watson CS, Kennedy MC, Bevington AR, Betts RA, Harrison S, Strattman K (2020) Rapid worldwide growth of glacial lakes since 1990. *Nat Clim Chang* 10(10):939–945
- Simoni A, Mammoliti M, Graf C (2012) Performance of 2D debris flow simulation model RAMMS. In: *annual international conference on geological and earth sciences GEOS*
- Somos-Valenzuela MA, Chisolm RE, Rivas DS, Portocarrero C, McKinney DC (2016) Modeling a glacial lake outburst flood process chain: the case of Lake Palcacocha and Huaraz, Peru. *Hydrol Earth Syst Sci* 20(6):2519–2543
- Uchida T, Nishiguchi Y, McArdell BW, Satofuka Y (2021) The role of the phase shift of fine particles on debris flow behavior: an numerical simulation for a debris flow in Illgraben, Switzerland. *Can Geotech J* 58(1):23–34
- Vicari H, Nordal S, Thakur V (2021) The significance of entrainment on debris flow modelling: the case of Hunnedalen, Norway. In: *Challenges and Innovations in Geomechanics: Proceedings of the 16th International Conference of IACMAG-Volume 2* 16, Springer, pp 507–514
- Vilímek V, Zapata ML, Klimeš J, Patzelt Z, Santillán N (2005) Influence of glacial retreat on natural hazards of the Palcacocha Lake Area, Peru. *Landslides* 2(2):107–115
- Vilímek V, Klimeš J, Emmer A, Benešová M (2015) Geomorphologic impacts of the glacial lake outburst flood from Lake No. 513 (Peru). *Environ Earth Sci* 73:5233–5244
- Wang Y, Hutter K, Pudasaini SP (2004) The Savage-Hutter theory: a system of partial differential equations for avalanche flows of snow, debris, and mud. *ZAMM-Journal of Applied Mathematics and Mechanics/Zeitschrift für Angewandte Mathematik und Mechanik: Applied Mathematics and Mechanics* 84(8):507–527
- Wegner SA, et al. (2014) Lo que el agua se llevó consecuencias y lecciones del aluvión de huaraz de 1941. nota técnica n° 7
- Westoby MJ, Glasser NF, Brasington J, Hambrey MJ, Quincey DJ, Reynolds JM (2014) Modelling outburst floods from moraine-dammed glacial lakes. *Earth Sci Rev* 134:137–159
- Worni R, Huggel C, Clague JJ, Schaub Y, Stoffel M (2014) Coupling glacial lake impact, dam breach, and flood processes: a modeling perspective. *Geomorphology* 224:161–176
- Zaginaev V, Ballesteros-Cánovas JA, Erokhin S, Matov E, Petrakov D, Stoffel M (2016) Reconstruction of glacial lake outburst floods in northern Tien Shan: implications for hazard assessment. *Geomorphology* 269:75–84
- Zaginaev V, Falatkova K, Jansky B, Sobr M, Erokhin S (2019) Development of a potentially hazardous pro-glacial lake in Aksay Valley, Kyrgyz range, Northern Tien Shan. *Hydrology* 6(1):3
- Zaginaev V, Petrakov D, Erokhin S, Meleshko A, Stoffel M, Ballesteros-Cánovas JA (2019) Geomorphic control on regional glacier lake outburst flood and debris flow activity over Northern Tien Shan. *Glob Planet Chang* 176:50–59
- Zheng G, Allen SK, Bao A, Ballesteros-Cánovas JA, Huss M, Zhang G, Li J, Yuan Y, Jiang L, Yu T et al (2021) Increasing risk of glacial lake outburst floods from future third pole deglaciation. *Nat Clim Chang* 11(5):411–417

G. Meyrat (✉) · **J. Munch** · **P. Bartelt**

WSL Institute for Climate Change, Extremes and Natural Hazards in Alpine Regions CERC, Davos, Switzerland
Email: guillaume.meyrat@slf.ch

A. Cicoira · **H. Frey**

Department of Geography, University of Zurich, Davos, Zurich, Switzerland

B. McArdell

WSL Institute for Forest, Snow and Landscape Research, Birmensdorf, Switzerland

C. R. Müller

Department of Mechanical and Process Engineering, ETH Zürich, Zürich, Switzerland